Mon. Not. R. Astron. Soc. **321**, 199–226 (2001)

Star cluster ecology – IV. Dissection of an open star cluster: photometry

Simon F. Portegies Zwart,[1]★† Stephen L. W. McMillan,[2] Piet Hut[3] and Junichiro Makino[4]
[1]*Massachusetts Institute of Technology, Cambridge, MA 02139, USA*
[2]*Department of Physics, Drexel University, Philadelphia, PA 19104, USA*
[3]*Institute for Advanced Study, Princeton, NJ 08540, USA*
[4]*Department of Astronomy, University of Tokyo, 7-3-1 Hongo, Bunkyo-ku, Tokyo 113-0033, Japan*

Accepted 2000 August 21. Received 2000 August 17; in original form 2000 May 22

ABSTRACT

The evolution of star clusters is studied using *N*-body simulations in which the evolution of single stars and binaries is taken self-consistently into account. Initial conditions are chosen to represent relatively young Galactic open clusters, such as the Pleiades, Praesepe and the Hyades. The calculations include a realistic mass function, primordial binaries and the external potential of the parent Galaxy.

Our model clusters are generally significantly flattened by the Galactic tidal field, and dissolve before deep core collapse occurs. The binary fraction decreases initially because of the destruction of soft binaries, but increases later because lower mass single stars escape more easily than the more massive binaries. At late times, the cluster core is quite rich in giants and white dwarfs. There is no evidence for preferential evaporation of old white dwarfs. On the contrary, the white dwarfs formed are likely to remain in the cluster. Stars tend to escape from the cluster through the first and second Lagrange points, in the direction of and away from the Galactic Centre.

Mass segregation manifests itself in our models well within an initial relaxation time. As expected, giants and white dwarfs are much more strongly affected by mass segregation than main-sequence stars.

Open clusters are dynamically rather inactive. However, the combined effects of stellar mass-loss and evaporation of stars from the cluster potential drive the dissolution of a cluster on a much shorter time-scale than if these effects are neglected. The often-used argument that a star cluster is barely older than its relaxation time and therefore cannot be dynamically evolved is clearly in error for the majority of star clusters.

An observation of a blue straggler in an eccentric orbit around an unevolved star or a blue straggler of more than twice the turn-off mass might indicate past dynamical activity. We find two distinct populations of blue stragglers: those formed above the main-sequence turn-off, and those which appear as blue stragglers as the cluster's turn-off drops below the mass of the rejuvenated star.

Key words: binaries: close – blue stragglers – stars: evolution – stars: mass-loss – open clusters and associations: general.

1 INTRODUCTION

Star clusters are remarkable laboratories for the study of fundamental astrophysical processes spanning the range of stellar evolution, from birth to death. Open clusters are relatively small (typically $\lesssim 10^4$ stars), young (generally $\lesssim 1$ Gyr old) systems found primarily in the Galactic disc. Roughly 1100 are known to lie within a few kiloparsecs of the Sun (Lyngå 1987). As a class, they afford us the opportunity to witness star formation and explore the complex evolution of young stellar systems. Since stars are born in star clusters and become part of the general Galactic population only when the parent cluster dissolves in the Galactic tidal field, it is of considerable interest to understand how this process occurs, on what time-scale it operates, and what are the detailed observable consequences of cluster evolution.

★ E-mail: spz@space.mit.edu
† Hubble Fellow.

At least as a first approximation, many star clusters are quite well characterized dynamically as pure *N*-body systems, in that there are few collisions or close encounters between stars, and the clusters themselves are relatively isolated in space. The same argument can be made for the evolution of the stars and binaries without interactions, which may also quite well explain the properties of open clusters. This simple picture rapidly becomes inadequate when two effects are combined – cluster evolution is actually an intricate mix of dynamics, stellar evolution and external (tidal) influences, and the subtle interplay between stellar dynamics and stellar physics makes for a formidable modelling problem. Of the many physical processes influencing cluster evolution, probably the most important are the effects of stellar evolution, the tidal field of the Galaxy, and the evolution and dynamics of binary stars. We present here a series of models in which all these effects are taken self-consistently into account.

The processes just mentioned are tightly coupled, complicating the evolution and making it difficult to isolate the importance of each individual effect. We refer to Meylan & Heggie (1997) for a recent review. Generally speaking, we can say that mass-loss from stellar evolution is of greatest importance during the first few tens of millions of years of cluster evolution, and may well result in the disruption of the entire cluster (cf. Chernoff & Weinberg 1990; Fukushige & Heggie 1995; Aarseth & Heggie 1998; Takahashi & Portegies Zwart 2000). If the cluster survives this early phase, stellar evolutionary time-scales soon become longer than the time-scales for dynamical evolution, and two-body relaxation and tidal effects become dominant. Ultimately, these effects cause the cluster to dissociate and the stars to become part of the general 'field' population of the disc.

There is strong observational evidence that star clusters contain substantial binary populations, quite possibly as rich as those found in the field (see Rubenstein 1997). The properties and numbers of observed cluster binaries cannot be explained by dynamical formation processes, such as three-body dynamics or two-body tidal capture (Aarseth & Lecar 1975). The majority must be primordial, i.e., formed together with the single stars at the cluster's birth. These observations are important for cluster dynamics, as a cluster's evolution depends strongly on its binary population and even a small initial binary fraction can play a pivotal role in governing cluster dynamics (Goodman & Hut 1989; McMillan, Hut & Makino 1990, 1991a,b; Gao et al. 1991; Hut et al. 1992; McMillan & Hut 1994). Binaries are also crucial to cluster stellar evolution. The possibility of mass transfer between binary components permits wholly new stellar evolutionary states to arise; in addition, the presence of binaries will enhance the rate of stellar collisions and close encounters, through the temporary capture of single stars and other binaries in three-body resonance encounters (Verbunt & Hut 1987; Portegies Zwart et al. 1998).

Until quite recently, dynamical models have tended to exclude binaries, for the good practical reasons that (1) binaries slow down the calculations dramatically and tend to induce numerical errors, and (2) their internal evolution is much more complicated than the evolution of single stars. However, it has also long been known that cluster models lacking adequate treatments of binary systems are of at best limited validity. In this paper we begin to address these limitations by performing calculations of open clusters containing substantial numbers of primordial binaries, with the goal of studying the mutual influence of stellar evolution and stellar dynamics in these systems – the 'ecology' of star clusters (Heggie 1992).

The first paper in this series (Portegies Zwart et al. 1997a, hereafter Paper I) quantified the effect of collisions on stellar evolution, and attempted to assess the corresponding changes in the stellar population. The stellar number density was held constant in these calculations, thus excluding the possibility of any interplay between the dynamical evolution of the cluster and collisions between stars. In the second paper in this series (Portegies Zwart, Hut & Verbunt 1997b, hereafter Paper II), the evolution of a population of primordial binaries was followed in time by tracking in detail the results of encounters between single stars and binaries. The assumption of constant stellar number density was relaxed in Portegies Zwart et al. (1999, hereafter Paper III), where the dynamical evolution of a star cluster (without primordial binaries) was followed in detail using *N*-body calculations.

This paper continues the process of relaxing the simplifying assumptions made in Paper I. As in Paper III, we calculate the dynamical evolution of our model system by direct (*N*-body) integration of the system, but now including both stars and binaries in the computational mix. Binary evolution is incorporated into the *N*-body treatment, accounting for changes in binary orbital parameters due to stellar mass-loss, supernovae, tidal forces between the stars, mass transfer from one star to its companion, general relativistic corrections, etc. Encounters between binaries and single stars and higher order encounters (between binaries and binaries, and between binaries and triples, etc.) are fully integrated, as are the orbits of the other stars in the *N*-body system. All changes in the stellar and binary population caused by stellar evolution are fed back into the dynamical evolution of the parent cluster, allowing stellar dynamics and the stellar evolution to be studied simultaneously and self-consistently.

As an initial case study, we concentrate here on open star clusters near the Sun (between ~6 and 10 kpc from the Galactic Centre), which are less than 1 billion years old, and which initially contain a few thousand (~2000–3000) stars, roughly half of them in binaries. Well-known clusters fitting this general description are the Pleiades, Praesepe and the Hyades (see Table 1). Such systems are small enough that multiple simulations can be performed in order to improve statistical coverage of their properties, yet they are large enough and old enough that both stellar evolution and stellar dynamics have had time to play significant roles in determining their present structure and appearance.

In an effort to close the gap between theoretical and observational studies of cluster structure, in this and subsequent papers we will attempt wherever possible to 'observe' our model clusters using techniques similar to those employed by observers. For this paper we have chosen to adopt a 'photometric' approach. Consequently, we present little detailed information about the binaries in our calculations. Binary properties will be discussed in depth in a 'spectroscopic' companion paper (Portegies Zwart et al., Paper V, in preparation, hereafter Paper V).

Section 2 discusses the choice of initial conditions and parameters for our model clusters. The results of the calculations are presented in Section 3, followed by Section 4, which compares our results with selected observations on a cluster-by-cluster basis. Section 5 compares our results with some previous studies in this area. We summarize our work in Section 6. Two appendices are included: Appendix A gives an overview of the terminology used throughout the paper, and Appendix B reviews the 'Starlab' software package, and the implementation and coupling of its two main constituents kira (the *N*-body integrator Section B1) and SeBa (the stellar/binary evolution program Section B2).

Table 1. Observed and derived parameters for several open star clusters with which our simulations may be compared. Subsequent columns give (3) the distance to the cluster (in pc), (4) the cluster age (in Myr), (5) the half-mass relaxation time (in Myr), (6) the total mass (in $M_\odot$), (7) the tidal radius (in pc), (8) the half-mass radius (in pc), and (9) the core radius (in pc). In cases where the parameters (relaxation time, mass, etc.) are not accessible in the literature, we calculate them; these entries are printed *in italics*. In most cases these numbers can be calculated using equation (A9) or equation (A10). Dashes and question marks indicate that we cannot derive these numbers. The final two columns contain information on the cluster stellar content. The column labelled $f_{s:b:t}$ indicates the number of single stars, binaries and triples (separated by colons). For clusters where the numbers are given directly by observations, the table gives the observed numbers of each system. If the binary fraction is derived by other methods, we give the relative fractions normalized to the number of single stars. The last column ($N_{bss:gs:wd}$) gives the number of observed blue stragglers, giants and white dwarfs, separated by colons.

name	ref.	d [pc]	t [Myr]	t_{rix}	M [$M_\odot$]	r_{tide}	r_{hm} [pc]	r_{core}	$f_{s:b:t}$	$N_{bss:gs:wd}$
NGC 2516	a	373	110	*220*	*1000*	*13*	2.9	–	16:6:?	6:4:4
Pleiades	b	135	115	150	∼1500	16	2–4	1.4	137:60:2	0:3:3
NGC 2287	c	655	160–200	–	≳*120*	6.3	–	–	1:0.6:?	3:8:3
Praesepe	d	174	400–900	*370*	1160	12	*3.5*	2.8	1:0.3:0.03	5:5:11
Hyades	e	46	625	*390*	500–1000	10.3	*3.7*	2.6	1:0.4:0	1:4:10
NGC 2660	f	2884	900–1200	*315*	≳400	*9.6*	4	*1.5*	1:0.3:?	18:39:?
NGC 3680	g	735	1450	*28*	≳100	4.3	1.2	*0.6*	44:25:0	4:17:?

References to the literature (second column) are: (a) Abt & Levy (1972); Dachs, J & Kabus (1989); Hawley et al. (1999). (Note: we interpret the quoted limiting cluster radius as the half-mass radius.) (b) Pinfield et al. (1998); Raboud & Mermilliod, (1998); Bouvier et al. (1997); (c) Harris et al. (1993); Ianna et al. (1987); Cox (1954). (d) Andrievsky (1998); Jones & Stauffer (1991); Mermilliod & Mayor (1999); Mermilliod et al. (1990); Hodgkin et al. (1999). (Note: we interpret the quoted central radius for the cluster as the half-mass radius.) (e) Perryman et al. (1998, and references therein); Reid & Hawley (1999); (f) Frandsen et al. (1989); Hartwick & Hesser (1971); Sandrelli et al. (1999). (g) Hawley et al. 1999; Nordström et al. (1997); Nordström et al. (1996), Data on numbers of white dwarfs were taken from Anthony-Twarog (1984) for Praesepe, from Koester & Reimers (1981) for NGC 2287, and from von Hippel (1998) for the other clusters. Data on various clusters are also available via Mermilliod's `WEBDA` online catalogue via `http://obswww.unige.ch/webda/`.

2 INITIAL CONDITIONS

In order to begin a simulation, a number of critical cluster parameters must be chosen: the mass, virial radius, tidal radius (or its equivalent), the initial mass function, and the initial distributions of binary spatial density and orbital properties. Table 1 presents an overview of observed parameters for some star clusters with similar total masses, stellar membership and half-mass radii. The ages of these clusters vary widely, from about 110 Myr (Pleiades) to over 1 Gyr (NGC 3680). Their core and half-mass radii suggest that they may be described approximately by King models (King 1966) with dimensionless depths in the range $W_0 \sim$ 4–6, where larger W_0 corresponds to higher central concentration.

We define our mass-scale by arbitrarily adopting a 'Hyades-like' model, in which the mass of the system at an age of 625 Myr is $\sim$1000 $M_\odot$. We then estimate the initial mass of a cluster by applying a number of corrections. We adopt the initial mass function for the solar neighbourhood described by Scalo (1986). Table 2 shows how the Scalo mass function evolves in time. Approximately 20 per cent of the initial mass is lost by purely stellar-evolutionary processes.

In addition to stellar evolution, dynamical evolution of the star cluster and the tidal field of the Galaxy also tend to consume (eject) cluster stars, at a rate of about 10 per cent per relaxation time (Spitzer 1987). With a current relaxation time for Hyades of about 400 Myr (see Table 1), we estimate that the amount of mass lost by dynamical processes up to an age of 625 Myr is similar to the mass lost to stellar evolution. Adding these numbers provides a conservative lower limit to the amount of mass lost by the star cluster. This limit is conservative, because we have neglected the interaction between stellar mass-loss and dynamical mass-loss. We therefore adopt an initial cluster mass of $M_0 \sim 1600\,M_\odot$. This is close to Weidemann (1993) estimate for the initial mass of Hyades (1800 $M_\odot$). We assume a Scalo (1986) initial mass function, with minimum and maximum masses of 0.1 and 100 $M_\odot$, respectively, and mean mass $\langle m \rangle \simeq 0.6\,M_\odot$. Our simulations are performed with 1024 single stars and 1024 binaries, for a total of 3096 (3k) stars and a binary fraction of 50 per cent.

Table 2. Number N_x of stars of type x and total mass M, from the Scalo (1986) initial mass function, evolved with SeBa. The calculation was performed with a population of 100 k stars, but the numbers are normalized to 1 k stars.

time [Myr]	0	100	200	400	600	800
ms	1024	1015	1008	996.7	988.3	982.1
gs	0	2.7	4.3	6.2	6.2	5.8
wd	0	3.0	8.5	17.6	26.0	32.7
ns	0	3.6	3.6	3.6	3.6	3.6
M [$M_\odot$]	624.4	562.3	541.5	517.6	501.1	490.6

Stars and binaries within our model are initialized as follows. A total of 2k single stars are selected from the initial mass function and placed in an equilibrium configuration in the selected density distribution (see Table 4). We then randomly select half the stars, and add a second companion star to them. The masses of the companions are randomly selected between 0.1 $M_\odot$ and the primary mass. For low-mass primaries, the mass ratio distribution peaks at unity, whereas the distribution is flat for more massive primaries. Once stellar masses are chosen, other binary parameters are determined. Binary eccentricities are selected from a thermal distribution between 0 and 1. Orbital separations a are selected with equal probability in $\log a$, with the lower limit set by the separation at which the primary fills its Roche lobe (RLOF) or at 1 $R_\odot$, whichever is smaller. The upper limit for the initial semimajor axis is taken at $10^6\,R_\odot$ (about 0.02 pc; Duquennoy &

Mayor 1991). When a binary appears to be in contact at pericentre, new orbital parameters are selected. Table 3 gives an overview of the various distribution functions from which stars and binaries are initialized.

We select initial density profiles from the anisotropic density distributions described by Heggie & Ramamani (1995) with $W_0 = 4$ and $W_0 = 6$, and refer to these models as W4 and W6, respectively, throughout this paper. The Heggie–Ramamani models are derived from King (1966) models, by taking into account the velocity anisotropy and non-spherical shape of the critical zero-velocity (Jacobi) surface of the cluster in the Galactic tidal field. (The classical King models have spherical boundaries.) Within the half-mass radius, the Heggie–Ramamani models are quite isotropic.

All models are started with a virial radius of $r_{\rm vir} = 2.5$ pc. For our adopted parameters, the initial cluster dynamical time-scale is then $t_{\rm c} \equiv (GM/r_{\rm vir}^3)^{-1/2} \sim 1.5$ Myr. Each cluster is assumed to precisely fill its Jacobi surface at birth. (Expressed less precisely, we could say that the limiting radius of the initial King model is equal to the Roche radius of the cluster in the Galactic tidal field.) Given the Oort constants in the solar neighbourhood, we find that the models with $W_0 = 6$ are somewhat farther ($\sim$12.1 kpc) from the Galactic Centre than is the Sun, while a model with $W_0 = 4$ is slightly closer ($\sim$6.3 kpc).

For a total cluster mass of 1600 $M_\odot$, the Lagrange points of our two standard clusters lie, respectively, at 14.5 pc ($W_0 = 4$) and 21.6 pc ($W_0 = 6$) from the cluster centre. A star is removed from a simulation when its distance from the cluster's density centre exceeds twice the distance from the centre to the first Lagrangian point.

Table 4 reviews the adopted parameters and initial conditions of our models. In order to improve statistics, we performed four calculations (labelled I to IV) for each set of initial conditions.

3 RESULTS

We now discuss the 'photometric' properties of our model clusters. As mentioned above, we defer the discussion of 'spectroscopic' properties, including details on the various types of binaries found in our simulations, to Paper V.

Table 3. Initial conditions for the stellar and binary population. The first column gives the parameter, and the second and third columns give the symbol and the distribution function, followed by the lower and upper limits adopted.

parameter		function	limits	
			lower	upper
primary mass	M	$P(M) =$ Scalo	0.1 $M_\odot$	100 $M_\odot$
secondary mass	m	$P(m) =$ const.	0.1 $M_\odot$	M
orbital separation	a	$P(a) = 1/a$	RLOF	10^6 $R_\odot$
eccentricity	e	$P(e) = 2e$	0	1

3.1 Global properties

Fig. 1(a) shows the mass of the cluster as a function of time for several models. In this figure, the 'total mass' of a model is simply taken to be the sum of the masses of all stars remaining within the N-body system. This gives the mass larger than the mass bound to the system, and probably also larger than the mass that the observers would derive. The dashed line gives the results from model W6-III. The two dotted lines show the mass evolution of two of the W4 models (upper line: model W4-II, lower line: W4-IV), illustrating the run-to-run variations in dynamical evolution (which are mainly the result of the difference in the initial total masses of the two models, caused by different random seeds).

Table 5 indicates the differences between the various line styles in Fig. 1(a), except for the dotted line which represent calculations with $W_0 = 4$. All lines listed are computed using exactly the same stellar masses as in model W6-III.

The two solid lines in Fig. 1(a) show (upper line) the total mass of an N-body system without stellar evolution, but otherwise with the same initial conditions as run W6-III, and (lower line) the total mass of stars, excluding stellar dynamics but including mass-loss by stellar evolution (with the same initial stellar masses as in model W6-III; see Table 5 for a review of the line styles). Mass-loss in the absence of stellar evolution is not linear with time, as one expects from an equal mass N-body system; the presence of a mass function causes heavier stars generally to be lost later, resulting in larger mass-loss at a later time. However, the loss rate of stars is roughly constant, and the curvature of the upper solid line in Fig. 1(a) demonstrates the strong effects of mass segregation and cluster dynamics.

The actual variation of the cluster mass (under the combined effects of stellar mass-loss and dynamical evolution) is larger than the sum of the two separate effects by about 50 per cent (see dashed line in Fig. 1a). The interplay between stellar evolution and stellar dynamics is especially important during the later stages of the evolution. The presence of primordial binaries has little effect on the evaporation rate of the clusters. The dot-dashed line gives the total mass of the same model, but without binaries – all stars in the initial mass function (including binary secondaries) are redistributed with the same density profile as model W6-III. As noted by McMillan & Hut (1994), primordial binaries have little effect on the overall rate at which mass is lost from the cluster.

Fig. 1(b) shows the masses of two model clusters (W6-III and W4-II), with different criteria for the limiting radius of the stellar system. The solid lines give the total mass in the N-body system (see also Fig. 1a), the dotted lines the total mass within the Jacobi surface, and the dashed lines the total mass within the Jacobi

Table 4. Initial conditions and parameters for the selected models. The columns give the model name, initial mass ($M_\odot$), number of stars, dimensionless central depth of the potential well (W_0), the distance from the Galactic Centre (kpc), the initial relaxation and half-mass crossing times (both in Myr), r_x, r_y, and r_z, the distances from the cluster centre to the Jacobi surface (so r_x is simply the Jacobi radius, $r_{\rm J}$; see Appendix A), and the virial, half-mass and core radius (all in parsec).

name	M [$M_\odot$]	N	W_0	$R_{\rm Gal}$ [kpc]	$t_{\rm rlx}$ [Myr]	$t_{\rm hm}$ [Myr]	$r_{\rm Jacob}$ [pc]			$r_{\rm vir}$	$r_{\rm hm}$ [pc]	$r_{\rm core}$
W4	1600	3k	4	6.3	109	4.07	14.5	9.7	7.2	2.5	2.14	0.83
W6	1600	3k	6	12.1	102	4.15	21.6	14.4	10.8	2.5	2.00	0.59

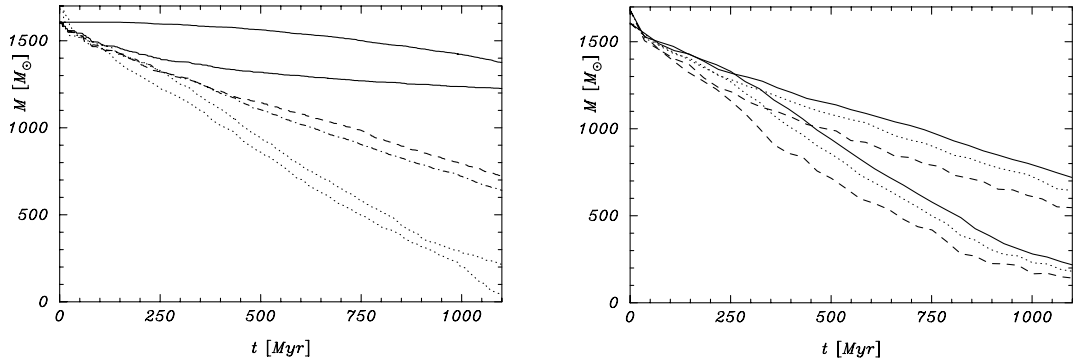

Figure 1. (a) Mass (in $M_\odot$) as a function of time (in Myr) for various models. The solid lines show the time-dependence of the total mass with (upper curve) stellar evolution suppressed, and (lower curve) without dynamical evolution. The dashed line is the total mass of model W6-III. The dot-dashed line is the total mass of a calculation with the identical mass function as in model W6-III, but all stars were single and redistributed in an identical density distribution. This line therefore gives the difference in a calculation with or without primordial binaries, but with all the other effects the same. The dotted lines represent the total mass of models W4-II (upper) and W4-IV(lower). (b) Various definitions of the cluster mass (in $M_\odot$) as functions of time for model W6-III (upper set of three lines) and model W4-II (lower set of lines). Solid lines represent the total mass in the *N*-body system, dotted lines the mass within the Jacobi surface, and dashed lines the total mass seen in projection within a distance r_J of the cluster centre.

Table 5. Overview of the variation in parameters for model W6-III in Fig. 1(a). The realization of the initial mass function was identical for all these models. Other parameters are as in Table 4. For each of these calculations some feature of starlab was switched on (+) or off (-); Kira (the *N*-body integrator), SeBa (the stellar and binary evolution model) and whether the calculation started with primordial binaries. Both dotted lines in Fig. 1(a) are computed using all model features of starlab, Kira, SeBa and with primordial binaries, but for an initial King model with $W_0 = 4$.

	Starlab		Primordial
line style	Kira	SeBa	binaries
upper solid	−	+	+
lower solid	+	−	+
dashes	+	+	+
dash-dots	+	+	−

radius of the cluster centre, as seen by an observer looking along the *y*-axis. The total mass in stars in the *N*-body system overestimates the mass of the cluster; the mass within the zero velocity surface may give a better measure of the mass one would observe in a real situation. The cluster mass within the Jacobi radius, viewed along the *x*-axis (towards the Galactic Centre), always lies between the solid and dotted lines; the corresponding mass viewed along the *z*-axis (from above the Galactic plane) lies between the dotted and the dashed lines. These trends are found in all models studied.

Fig. 2(a) presents the observational equivalent of Fig. 1(b), showing the total M_V magnitude of the W6 models at various times. The spread in M_V is caused by the intrinsic differences between runs – initial conditions, run-to-run variations and fluctuations due to the small numbers of giants, which dominate the total magnitude. Note that, for technical reasons, the output intervals are not the same for the four calculations shown here.

Fig. 2(b) plots the integrated $B - V$ colour of the cluster as a function of time. The initial colour of all models is confined to a small range between $B - V \simeq -0.15$ and -0.28, but rapidly grows to larger values with a larger spread: $B - V \simeq 0.1$–0.4 at 50 Myr and $B - V \simeq 0.5$–0.8 at 500 Myr. As in Fig. 2(a), the intrinsic spread is caused by the presence of a relatively small number of giant stars. The increase in the colour index indicates that the cluster gets redder with age, which is mainly due to the loss of the massive blue stars and the formation of red giants. The colour variation of the W4 models is similar.

Fig. 3 shows how the radii of models W4 and W6 evolve with time. All stars in the *N*-body system are taken into account in calculating the Lagrangian radii. The outer radii therefore expand much more than they would do if only stars within the Jacobi surface were considered. The W6 models experience core collapse between $t = 100$ and 150 Myr, and somewhat earlier for the W4 models, but neither is very deep. This shallow core contraction phase demonstrates the importance of a large-mass spectrum, stellar mass-loss and, to a lesser extent, binary heating to the dynamical evolution of these systems; mass segregation, for example, also plays an important role here (see Fig. 5). A comparable model with primordial binaries and without stellar evolution would experience core collapse (McMillan et al. 1990, 1991a), even in the presence of a Galactic tidal field (McMillan & Hut 1994).

In contrast to the W6 radii shown in Fig. 3(a), the Lagrangian radii of model W4-II (Fig. 3b) expand for about 300 Myr, and subsequently shrink. The decrease in Lagrangian radii at late times is an indicator of cluster evaporation. As the cluster dissolves in the Galactic tidal field, its tidal radius decreases, accelerating the dissolution and causing the Lagrangian radii to decrease. The W6 clusters show the same behaviour, but at somewhat later times. We show the result of a single W4 model to illustrate the intrinsic fluctuations within a single *N*-body run.

Finally, Fig. 4 shows the half-mass relaxation time (equation A9) as a function of time for models W6-III (solid line) and W4-II (dashed line). Note that the relaxation time peaks around the cluster's 'half-life' epoch: 750 and 400 Myr for models W6-III and W4-II, respectively. Consequently, estimates of the present-day relaxation time of observed open clusters may provide poor indicators of the dynamical age of the stellar system. The often-used argument that a star cluster is barely older than its relaxation time and therefore cannot be dynamically evolved is clearly in error for the majority of star clusters (see also McMillan & Hut 1994).

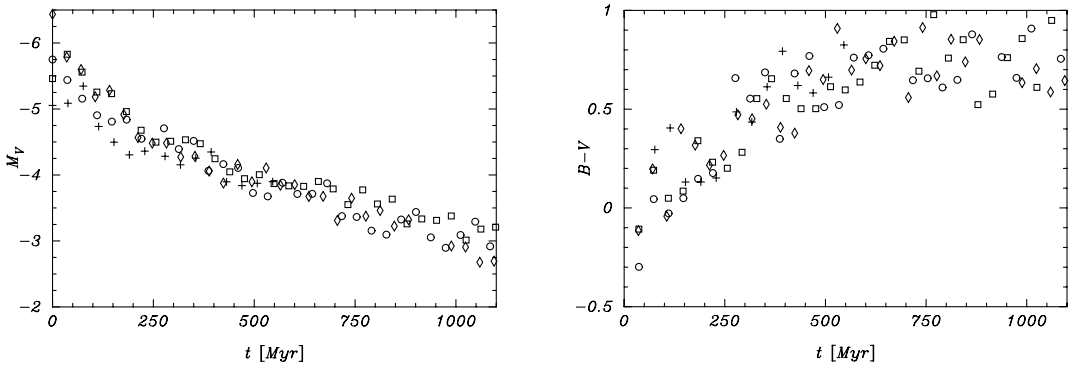

Figure 2. (a) Integrated M_V magnitude as a function of time of the four W6 models (pluses, circles, squares, and diamonds give the data for the models I–IV). (b) Integrated $B - V$ colour as a function of time for the W6 models.

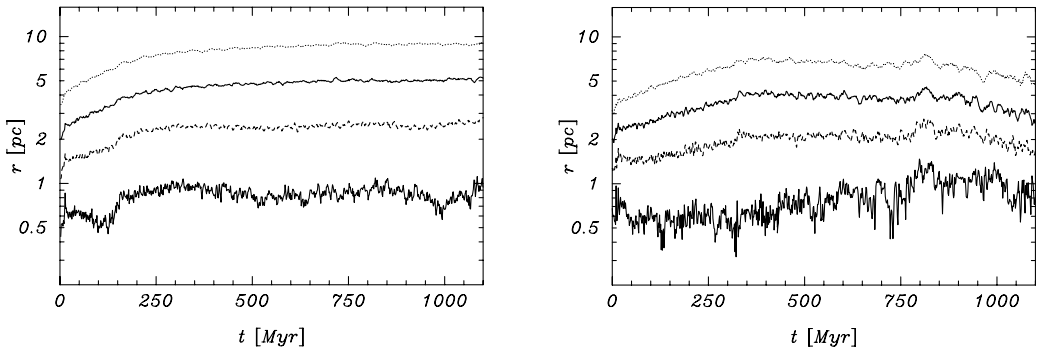

Figure 3. Lagrangian radii (in pc) as functions of time. The data in (a) represent the mean of the four W6 runs, and those in (b) model W4-II. From top to bottom, the radii contain the following mass fractions: 75 per cent (dots), 50 per cent (upper solid), 25 per cent (dashes) and 5 per cent (lower solid).

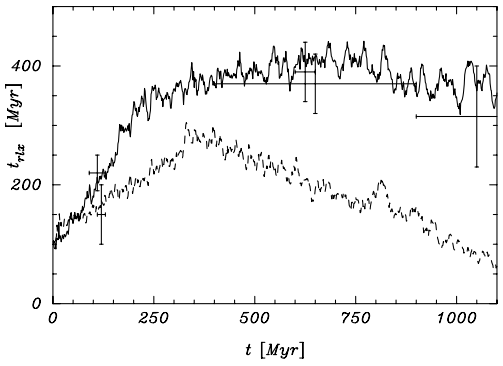

Figure 4. Half-mass relaxation time as a function of time for the models W6-III (solid) and for model W4-II (dashes). The error bars indicate the computed relaxation times for the observed star clusters from Table 1. (Confidence intervals are not listed in the table.)

3.2 Mass segregation

The effect of mass segregation is clearly visible in Fig. 5(a), which shows the mean mass $\langle m \rangle$ of stars within the 5, 25, 50 and 75 per cent Lagrangian radii as functions of time, averaged over the four W6 models. The initial increase in the mean mass within the inner 5 per cent Lagrangian radius is the result of mass segregation. The value of $\langle m \rangle$ in the cluster centre decreases again after about 100 Myr, when the most massive stars leave the main sequence and lose most of their mass on the asymptotic giant branch. For the remainder of the calculation, $\langle m \rangle$ stays more or less constant in each Lagrangian zone, but with a significantly higher value in the inner zones.

Fig. 5(b) shows the evolution of the mean mass $\langle m \rangle$, in model W4-II. Mass segregation in this model proceeds on a longer time-scale than in the W6 models, but the cluster dissolves on a shorter time-scale. Near the end of the cluster lifetime the mean mass in the outer regions increase, caused by the preferential loss of the lower mass stars by evaporation; the more massive stars have greater difficulty in climbing out of the potential well.

Fig. 6 shows the mean mass-to-light ratio for the W6 models. Except for the first few million years, the mass-to-light ratio in the cluster core is always substantially smaller (and noisier) than that in the halo, as mass segregation causes the most massive (i.e., brightest) stars to sink rapidly to the cluster centre. The general increase in mass-to-light ratio with time is the result of stellar evolution. The occasional dips in the mass-to-light ratio are caused by individual red giant stars; most of these dips occur in the core, where mass segregation causes the giants to accumulate. We can reduce this 'noise' considerably by averaging over the four W6 calculations, but the effect remains visible.

Fig. 7(a) shows the radial stellar distribution in the W6 models at various epochs. The cluster expands as it ages. The binaries (dotted lines) closely follow the distribution of the single stars for the first 100 Myr, but become more centrally concentrated at later epochs. Mass segregation is also clearly visible if we compare the radial distributions of low-mass (faint) stars with the more massive (bright) stars (Fig. 7b). Stars with $L > 0.5\,L_\odot$ are clearly more centrally concentrated than the mean cluster star, while giants (although there are only a few) are even more strongly concentrated in the cluster centre.

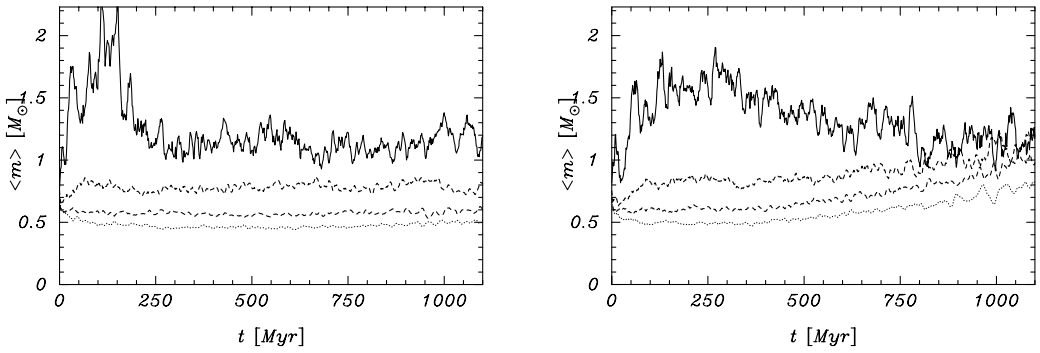

Figure 5. (a) and (b) The mean mass $\langle m \rangle$ of model W6-III (a) and W4-II (b), as functions of time. The data have been smoothed over time intervals of 8.8 Myr. From top to bottom, the lines represent the mean mass within the 5 per cent (solid), 25 per cent and 50 per cent (dashes) and 75 per cent (dots) Lagrangian radii (see Fig. 3 for the corresponding radii.)

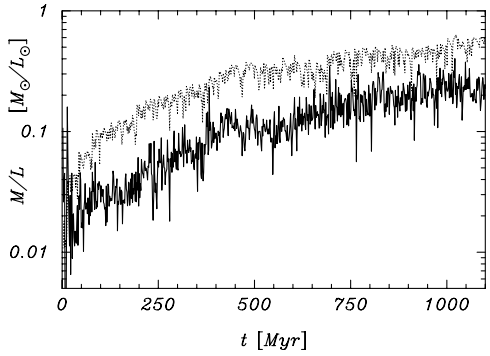

Figure 6. The mean mass-to-light ratio for models W6-I to IV, within the 5 per cent (solid) and 75 per cent (dots) Lagrangian radii.

Mass segregation can also be observed in the cluster's mass and luminosity functions. Fig. 8(a) shows global mass functions for all single stars and binary primaries for the W6 models at birth and at $t = 600$ Myr. The global mass function of the cluster is affected only slightly by stellar evolution and mass segregation. However, the mass function at $t = 600$ Myr for stars in the inner part of the cluster (dot-dashed line) is clearly different from the global mass function at that time.

The white dwarfs are more centrally concentrated than stars with luminosity $>0.5\,L_\odot$ and slightly less concentrated than the giants (see Fig. 7b). This is caused by the progenitors of the white dwarfs, the giants, being centrally concentrated, while after their envelopes are shed they have masses comparable to the mean cluster stars. Segregating outwards takes more time than sinking inwards, and at the same time more white dwarfs are produced in the cluster centre (see the end of this section for more details).

Fig. 8(b) shows the luminosity functions (in M_V) for stars (including binaries) in models W6 at zero age, 600 Myr and at an age of 1.1 Gyr. Note that the luminosity function at the later time shows a *larger* faction of bright stars. The reason is two-fold: (1) stellar evolution has removed only the most massive stars by this time, while mass segregation has concentrated the remaining massive (bright) stars in the cluster core, at the same time causing the lower mass stars to escape, and (2) the heaviest stars turn into giants, which for older (lighter) stars are much brighter than main-sequence stars, whereas for younger (heavier) stars, the difference in brightness between giant and main-sequence stars is much smaller. Near the end of the clusters' lifetime (solid lines in Fig. 8) the enormous overabundance of stars with a mass of 0.6–0.8 $M_\odot$ is caused by the large number of white dwarfs in the cluster; a population of main-sequence stars with the same mass would lead to an excess of stars with absolute visual magnitudes 8.6 – 6.4 in Fig. 8(b). The populations of giants and white dwarfs in the later stage of the cluster are discussed in more detail in Section 6.6. The excess of stars with masses up to $2\,M_\odot$ in Fig. 8(a) is caused mainly by main-sequence stars which have sunk in the cluster potential. These stars also gives rise to an excess of bright stars in Fig. 8(b).

The W4 models are more strongly affected by mass segregation (not shown, but see Section 4). In part, this is caused by the more rapid evaporation of these models compared to the W6 models.

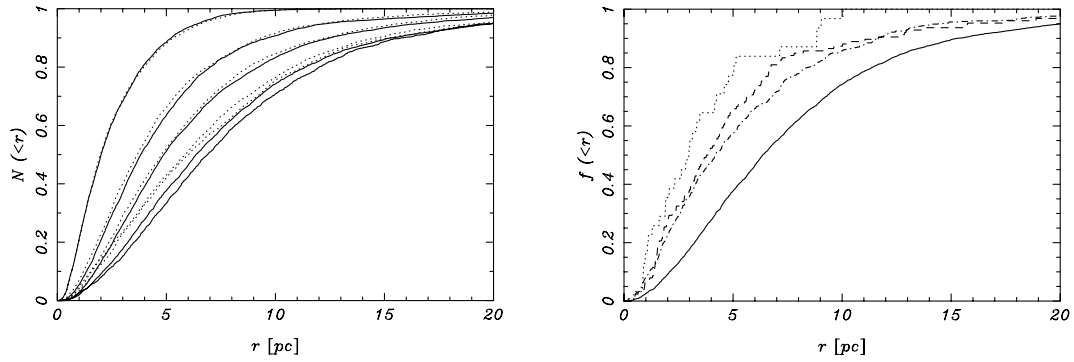

Figure 7. (a) Cumulative distribution of single stars (solid lines) and binaries (dotted lines), averaged over the four W6 models, at (upper left to lower right) $t = 0$, 100, 200, 600 and 800 Myr. (b) Cumulative distribution of various stellar populations for the four W6 runs at an age of 600 Myr. Solid line: the distribution of all stars (see also the appropriate solid line in panel (a); dot-dashed line: stars with $L > 0.5\,L_\odot$; dashed line: white dwarfs; dotted line: (sub)giants.

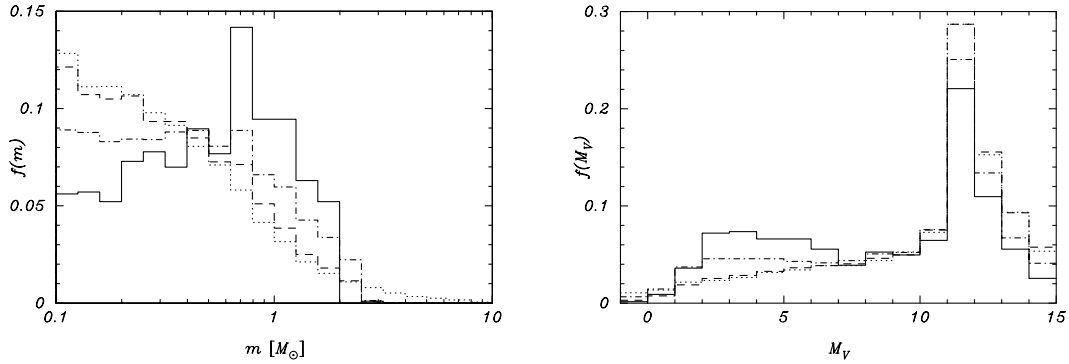

Figure 8. Mass function (a) and luminosity function (b) for model W6. The dotted lines give the $t = 0$ distributions, and the dashed lines give the distributions at $t = 600$ Myr (averaged over all models). The dot-dashed lines are the mass (luminosity) functions for stars within 3.4 pc (the half-mass radius for W6 models at $t = 600$ Myr) of the density centre [for (b) in projection, as viewed along the x axis]. The solid line gives the mass function of the W6 models within the cluster $r_{\rm hm}$ [projected again for (b)] at an age of 1100 Myr.

This is consistent with the findings of Takahashi & Portegies Zwart (2000), who noted that clusters which are close to complete disruption contain a higher fraction of high-mass stars.

3.3 Hertzsprung–Russell diagrams

Fig. 9 shows a time sequence of Hertzsprung–Russell diagrams for model W6-III. The youngest Hertzsprung–Russell diagram (200 Myr) already shows a white dwarf sequence. Note the densely populated 'binary sequence' ~0.75 mag above the zero-age main-sequence (ZAMS). One of the objects in the middle panel (close to but just above the turn-off) is a blue straggler; the other two are binaries (see also Fig. 11). The objects immediately to the left of the main sequence (the two points in the 600 Myr diagram at $B - V \sim 1.18$ and the single point at $B - V \sim 0.5$, $V = 8$) are binaries containing a mass-transfer remnant (a helium star) and a main-sequence star which has accreted part of its companion's envelope. Farther to the blue (between $B - V = 0$ and 0.8), but to the right of the white dwarf sequence, are binaries consisting of two white dwarfs (several are indicated with a '●' in the 600- and 1100-Myr diagrams). In the bottom panel a break and discontinuity in the ZAMS is visible near $B - V = 0.4$ and at $V \simeq 4$. This is an artefact of the stellar evolution fitting formulae given by Eggleton, Tout & Fitchett (1989), and appears when the envelope of a main-sequence star becomes convective.

Fig. 10 shows Hertzsprung–Russell diagrams for the inner, middle and outer regions of the combined W6 models at an age of about 600 Myr, and illustrates the effect of mass segregation. Each diagram contains about 2000 objects. The slight 'fuzziness' near the main-sequence turn-off is the result of variations in output times between individual simulations, which cause the combined diagram to have a small spread in stellar ages. About one-quarter (one run) of the stars come from a slightly younger cluster with an age of about 550 Myr.

The Hertzsprung–Russell diagrams of the inner and outer parts of the cluster show significant differences due to mass segregation. The inner HRD has a clear excess of (sub)giants and white dwarfs relative to the HRD at the half-mass radius or that in the halo. The population of single white dwarfs and binaries consisting of two white dwarfs is richest in the top panel of Fig. 10, and their number decreases in the lower panels (see Section 6.6 for discussion). Also, the turn-off region is more heavily populated in the inner HRD than in the others. Striking also is the lack of a clear binary sequence in the outer Hertzsprung–Russell diagram. The bottom of the main sequence is less clearly affected by mass segregation.

3.4 Blue stragglers

The (small) numbers of blue stragglers do not depend strongly on the particular region of the cluster under study. We count four blue stragglers in the inner Hertzsprung–Russell diagram, and one and two in the middle and outer frames of Fig. 10, respectively. These numbers are fairly typical of our simulated clusters, and also quite typical for the numbers observed (see Table 1). Fig. 11 presents a graphical representation of the blue stragglers in model W6-III. (A main-sequence star is identified as a blue straggler as soon as its mass exceeds the turn-off mass for that epoch.)

Most blue stragglers are the result of mass transfer in a close binary. In about half of all cases (37 out of 76 blue stragglers formed in all calculations performed), the mass transfer is unstable, leading to a merger. Blue stragglers formed from a stable phase of mass transfer are generally accompanied by a white dwarf or helium star (the young remnant of mass transfer; see Fig. 11), causing the blue stragglers to lie slightly blueward of the turn-off in the Hertzsprung–Russell diagram (see Section 3.3).

Three blue stragglers formed via collisions in which a third star interacted with a binary, leading to a blue straggler accompanied by a main-sequence star in an eccentric orbit. In each of these cases, the binary components coalesced and the third star was captured into the binary. Observing a blue straggler in an elliptical orbit around a stellar (main-sequence) companion would provide strong evidence for such dynamical interactions in star clusters (see Portegies Zwart 1996).

In none of our calculations was a blue straggler with more than twice the turn-off mass formed, i.e., there were no collisions between three or more stars. A discovery of a blue straggler with a mass more than twice the turn-off mass would provide strong evidence for effects of stellar dynamics, although one could imagine a primordial triple to get into a common-envelope situation in which all three stars spiral in to a triple merger. In Paper III we found runaway collisions between more than two stars in the simulations of dense stars clusters without primordial

binaries. These results, however, are applicable for a different range of initial conditions, as they studied the dense and young central star clusters R 136 in the 30 Doradus region of the Large Magellanic Cloud.

Many blue stragglers experience mass transfer or a collision long before actually being classified as blue stragglers by our criterion (i.e., exceeding the turn-off mass). In most of these cases, one or more phases of mass transfer (stable or unstable, or even accretion from the stellar wind of a companion) has rejuvenated one of the stars in a close binary system (see Appendix B). As the cluster ages, the star remains behind on the main sequence, and eventually becomes identifiable as a blue straggler (see also Paper II). This is illustrated in Fig. 11 (the two long tracks with $m \sim 2$ and the track near $m \sim 3$).

A blue straggler which was rejuvenated long ago may show no trace of the event that caused its rejuvenation. Apart from residing above the turn-off, the star may appear completely normal; anomalous atmospheric abundances will have had sufficient time to mix with the stellar interior. In addition, if the blue straggler is rejuvenated only a little, the maximum distance on the Hertzsprung–Russell diagram between the cluster turn-off and the blue straggler will be very small; such a star may remain unidentified as a blue straggler. This may happen if mass transfer is unstable but does not lead to a merger, or if a binary is too wide for Roche lobe overflow, and the blue straggler is rejuvenated by accreting a small portion if its companion's stellar wind.

The lifetime of a blue straggler depends on the epoch at

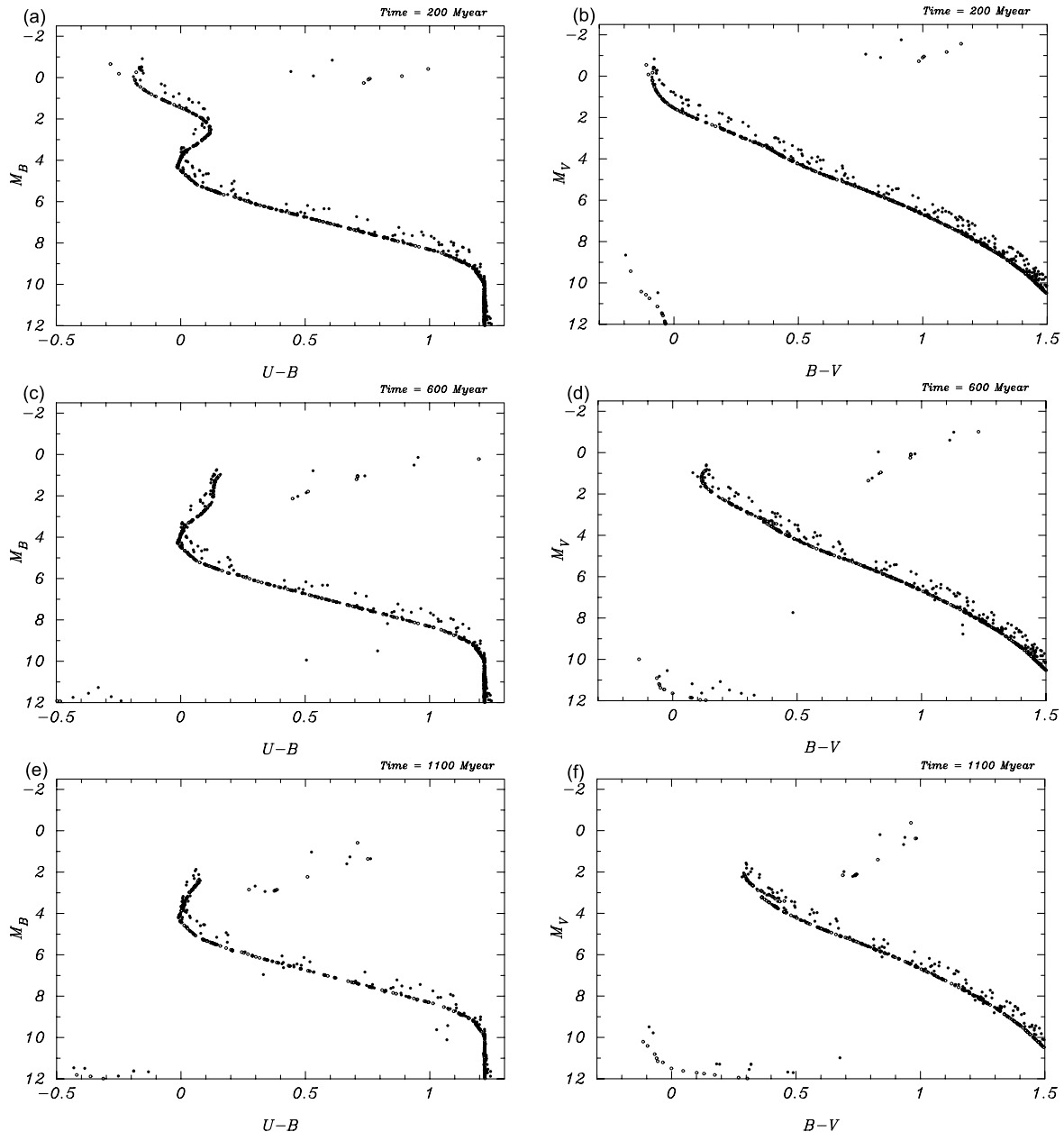

Figure 9. Hertzsprung–Russell diagram of all stars in model W6-III at ages of 200 Myr $U-B$ in the left-hand panels and $B-V$ in the right-hand panels (upper panels; 1983 objects), 600 Myr (middle; 1603 objects), and 1100 Myr (lower panels; 1009 objects). Single stars are indicated with open circles, and binaries with filled circles.

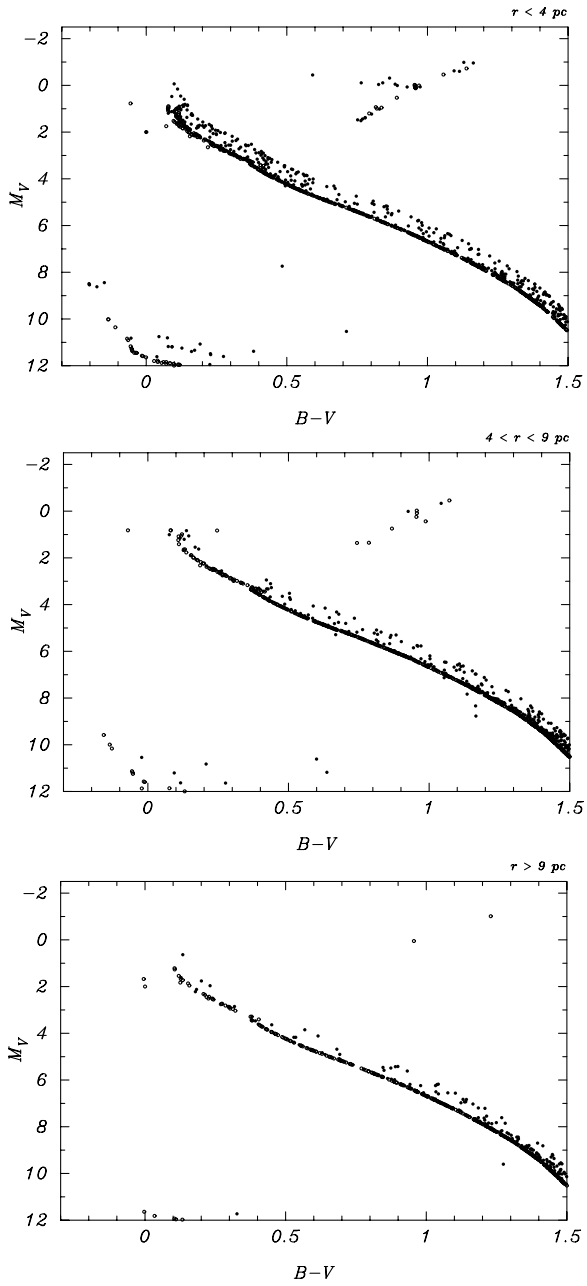

Figure 10. Hertzsprung–Russell diagrams of the combined W6 models at an age of about 600 Myr. The upper panel shows the innermost (non-projected) 4 pc (2004 objects), the middle panel stars between 4 and 9 pc from the cluster centre (2058 objects), and the bottom panel stars more than 9 pc from the centre (2039 objects). Single stars are indicated with open circles, and binaries with filled circles.

which it formed. Blue stragglers that form later are generally products of lower mass stars, and tend to live longer than blue stragglers that formed early in the evolution of the stellar system.

3.5 Isophotes

Fig. 12 shows a series of isophotes, as seen from various directions, for model W6-III at an age of 600 Myr. The Galactic

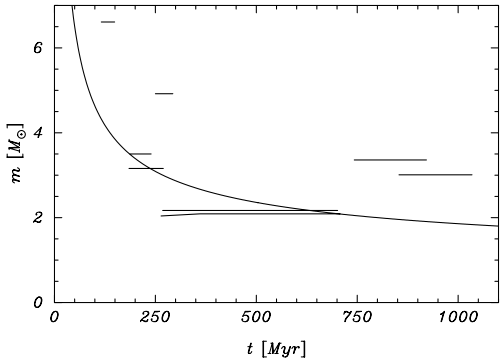

Figure 11. Blue stragglers in model W6-III. The solid curve gives the turn-off mass (in $M_\odot$) as a function of time (in Myr). The horizontal lines represent the tracks of the blue stragglers in model W6-III. The tracks start when the star is rejuvenated (see Appendix B), and stop when the blue straggler leaves the main sequence.

Centre is located to the $-x$ direction (at a distance of 12.1 kpc – see Table 4), and z points toward the North Galactic Pole. While the cluster is barely flattened at birth,[1] by 600 Myr the cluster is significantly flattened by the Galactic tidal field. As expected, the flattening is greatest along the z-axis, and also noticeable in the y-direction.

Fig. 13 shows images of model W6-III at three different moments in time. The images are created using a ray-tracing technique.

3.6 Escaping stars

Stars escaping from the cluster are lost primarily near the first and second Lagrange points. Figs 14 and 15 show the positions and projected velocities of the first 100 escapers from the system, and the 100 stars which escaped between $t = 550$ and 650 Myr. The left and right panels show, respectively, projections on to the x-z and x-y planes. The first and second Lagrange points lie on the x-axis, at distances of $\sim$20 pc ($t = 0$) and $\sim$17 pc ($t \sim 600$) from the cluster centre. The small overall rotations of escapers evident in the x-y projections are consequences of the Coriolis force acting on stars in the rotating frame of reference in which we perform the simulations. The high-speed escapers with roughly isotropic velocities in Fig. 14 are escaping neutron stars, which receive high kick velocities on their formation. They are absent in Fig. 15, as the cluster is by that time too old for supernovae to occur (except for type Ia supernovae).

The main differences between Figs 14 and 15 are (1) the considerably larger spread in velocities, (2) the larger extent in z of the region over which stars are lost, and (3) the higher speeds of escaping stars at the earlier epoch. These differences are readily explained by a combination of effects; the evolution of the cluster in the Galactic tidal field, the presence of primordial binaries and the formation of neutron stars. As the cluster ages it becomes less massive and the Galaxy's gravitational pull becomes relatively stronger. The tidal radius shrinks and the cluster velocity

[1] This is simply a consequence of the fact that only the outermost parts of the cluster, near the Jacobi surface, show significant flattening, and these are initially very sparsely populated. Only when cluster evolution drives many stars out to the Jacobi radius does the flattening become readily apparent.

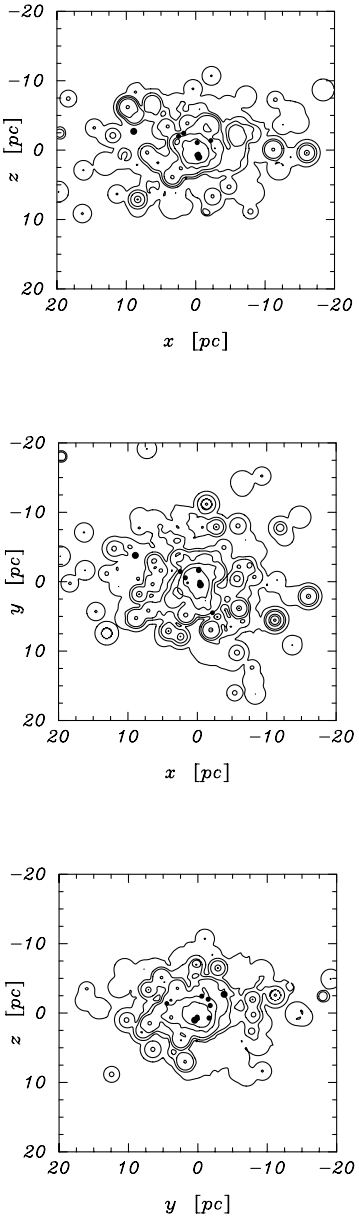

Figure 12. Isophotes in M_V for model W6-III at a cluster age of 600 Myr. The three panels present views along the three coordinate axes. The 10 (sub)giants are plotted as dots with size proportional to magnitude (and are excluded from the isophotes). The brightest region in the continuum plot has a surface brightness of $-2.2\,\mathrm{mag\,pc^{-2}}$. Contours are plotted at -0.86, 0.34, 1.6, 2.8, 4.1 and $7.8\,\mathrm{mag\,pc^{-2}}$. Stars are assigned a Gaussian point spread function with a dispersion of 0.35 pc.

dispersion decreases, so the speed of escaping stars and their distances above or below the Galactic plane also decrease. The older cluster also lacks massive stars, and therefore no stars are ejected via supernova explosions. The shallow core collapse during the first 100 Myr results in increased binary activity, which also contributes to the higher stellar ejection speeds at the earlier time.

3.7 Stellar populations

Tables 6 and 7 present, for several cluster ages, the numbers of single stars and binaries by generic stellar types. The numbers are averaged over the calculations performed for each set of initial conditions, chosen with a different random seed from the same probability distribution. Table 8 gives the same data for a population of evolving binaries without dynamics, calculated using SeBa (see Appendix B).

Overall, the evolutionary differences in the populations of single stars and binaries between models W6 and W4 are quite small. Clearly, as already noted, the W4 clusters evaporate more rapidly (Fig. 1), resulting in a generally more rapid decrease in the numbers of both stars and binaries. A more significant difference between Tables 6 and 7 is the larger numbers of white-dwarf binaries in the W4 models compared to other stellar types. Table 8 presents the stellar and binary properties of an evolving population of isolated binaries. The differences between these binaries and the dynamically evolving population is considerable.

Table 9 gives the fractions of various types of stars and binaries in the dynamical calculations, relative to the corresponding numbers from the population synthesis studies. The latter are normalized to the same numbers of single main-sequence stars and main-sequence binaries as in the initial dynamical calculations. (This normalization is employed here to show trends which are hard to see in the Tables 6, 7 and 8.) Neutron stars are omitted from the comparison because the differences are directly obvious: neutron stars escape from open star clusters, but they are retained in the non-dynamical models; black holes and binaries which contain two giants or a giant and a white dwarf are omitted because of their small numbers.

Although the numbers of single giants and white dwarfs are also rather small, a trend is clearly visible: single white dwarfs and dwarfs in binaries are more abundant at later stages in the dynamical calculations, especially for the W4 models. The basic reason for this overabundance of white dwarfs and giants is their larger mass, which makes them more likely to be retained by the cluster. White dwarfs experience a complex evolutionary path within the stellar system, their progenitors being among the most massive objects while on the main sequence and the giant branch, but the white dwarfs having masses comparable to the mean once their envelopes are lost. White dwarfs are therefore preferentially formed in the cores of star clusters. Once the white dwarf is formed, it is hard to extract it from the core. These effects are more pronounced in smaller clusters ($t_{\rm rlx} \lesssim 1\,\mathrm{Gyr}$). At a greater age the W4 models have a higher fraction of white dwarfs than the W6 models. This is a result of the smaller relaxation time of the W4 models which causes low-mass main-sequence stars to escape more easily; the cluster therefore becomes more rich in stars which have more difficulty to escape.

The number of contact main-sequence binaries [ms, ms] drops in the dynamical models, whereas in the purely binary evolution models their number remains roughly constant. In the dynamical models, contact binaries easily merge when they become perturbed by the close encounter of another star or binary, whereas in the binary population synthesis such binaries merge only when one of the stars leaves the main sequence (see Section B2).

4 COMPARISON WITH OBSERVATIONS

4.1 The Pleiades

Fig. 16 shows the M_I-magnitude luminosity function for the inner part of the Pleiades cluster (Hambly & Jameson 1991), and compares it with our model luminosity functions at 100 Myr.

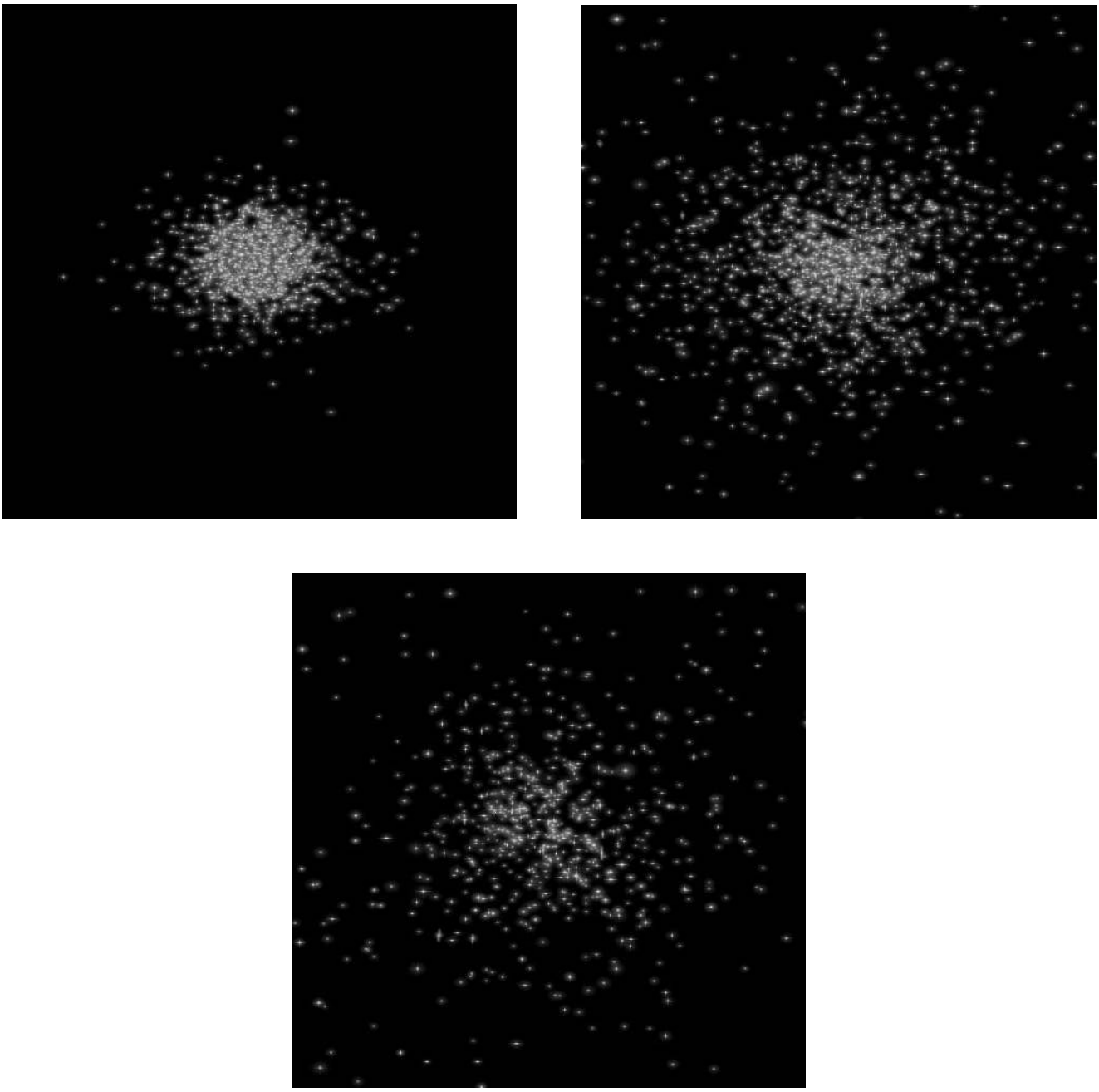

Figure 13. Visualization of model W6-III at zero age (top image), at an age of 622 Myr, and at an age of 1512 Myr. Images were created using a ray-tracing technique.

The best fit between the observed and model luminosity functions is obtained for the stars within the half-mass radius. This suggests that some mass segregation has already occurred in this cluster. Raboud & Mermilliod (1998) also find evidence for mass segregation in this cluster. Our luminosity function has too many bright stars, and to make a reasonable fit we have to exclude stars with $M_I < 4.5$ from the sample or, as is done in Fig. 16, lift the cumulative luminosity function with the number of brightest stars which are excluded in the sample by Hambly & Jameson (1991).

The Pleiades is flattened, with an observed ellipticity $\epsilon \equiv (1 - b/a)$ of 0.17. Taking into account the orientation of the cluster in the tidal field of the Galaxy, Raboud & Mermilliod (1998) derive an intrinsic ellipticity of almost 0.3 (see also van Leeuwen, Alphenaar & Brand 1986), comparable to what we find in our models (see Fig. 12) by comparing the distance to the Jacobi surface along the z-axis with the distance to L_1: $\epsilon \simeq 1 - r_z/r_{\rm J}$.

4.2 Praesepe

Fig. 17 shows the M_R-magnitude global luminosity function for the W6 clusters at birth and at 800 Myr, and compares that with the observed luminosity function for Praesepe reported by Hambly et al. (1995a,b), which is shown as filled circles with error bars.

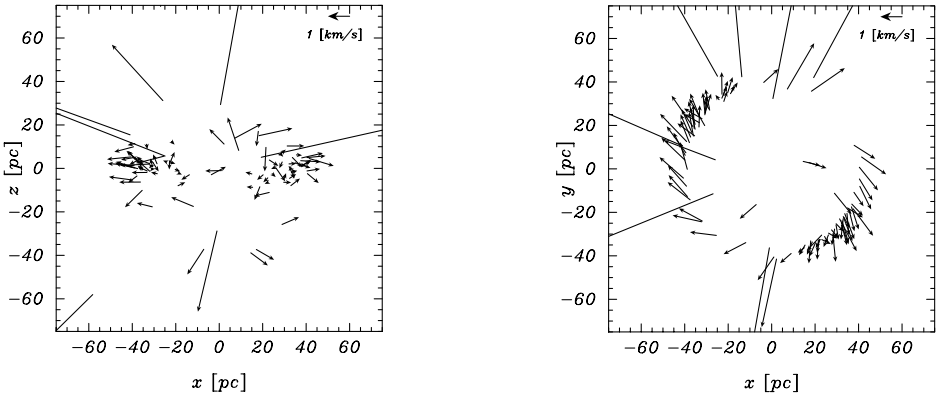

Figure 14. Vector diagram of the first 100 ($t < 218$ Myr) stars escaping from model W6-III. Projections on to the *x*-*z* plane and the *x*-*y* plane are shown. A velocity scale is shown in the upper right corner.

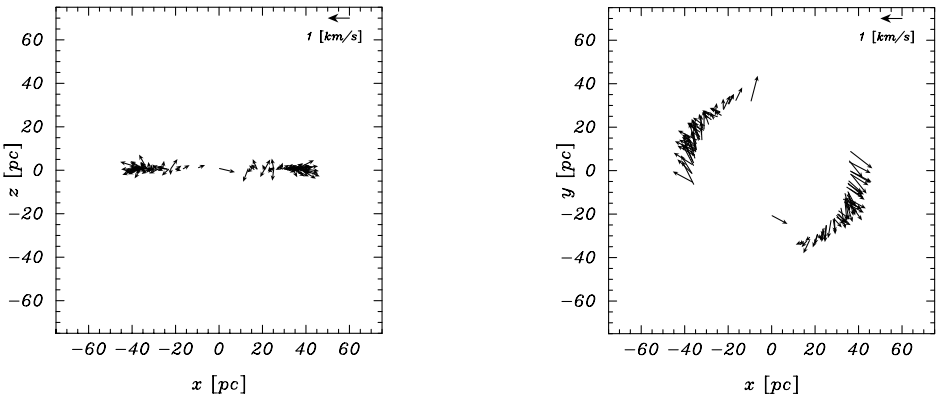

Figure 15. As for Fig. 14, but for the 100 stars escaping from model W6-III between $t = 550$ and 650 Myr.

Table 6. Stellar and binary types in the W6 models at various times. Binaries which contain two main-sequence stars are identified as (ms, ms), (ms, gs) contain a main-sequence star and a giant, (gs, gs) contains two giants, (gs, wd) contains a giant and a white dwarfs, and (wd, wd) contains two white dwarfs. A bracket indicates the binary component which fills its Roche lobe and is in a state of mass transfer to its companion star; binaries with neutron stars or black holes are omitted. The bottom row gives the binary fraction.

time [Myr]:	0	100	200	400	600	800
ms	1024	1174	1144	1038	914.5	678.0
gs	0	4.0	4.8	6.3	6.0	6.0
wd	0	6.0	11.8	26.5	32.5	35.0
(ms, ms)	1024	907.9	869.0	788.7	700.0	606.5
[ms, ms]	0	5.2	4.3	3.9	3.3	2.5
(ms, gs)	0	0.5	3.0	2.0	4.3	3.7
(ms, wd)	0	1.3	3.0	6.8	8.8	12.7
(gs, gs)	0	0.0	0.5	0.3	0.3	0.3
(gs, wd)	0	0.5	0.5	0.8	1.5	2.7
(wd, wd)	0	0.0	1.5	4.3	6.0	10.0
$f_{\rm bin}$	0.5	0.436	0.432	0.430	0.432	0.470

Table 7. Stellar and binary types in the W4 models.

time [Myr]:	0	100	200	400	600	800
ms	1024	1249	1174	964.0	604.5	164.0
gs	0	3.5	5.3	9.3	9.5	7.5
wd	0	5.3	11.8	25.8	33.5	31.0
(ms, ms)	1024	857.3	796.7	598.0	351.5	197.0
[ms, ms]	0	6.0	5.1	3.5	2.1	1.1
(ms, gs)	0	0.8	3.0	1.5	2.5	3.0
(ms, wd)	0	2.3	2.8	3.0	5.5	6.0
(gs, gs)	0	0.0	0.0	0.3	0.0	1.0
(gs, wd)	0	0.5	0.8	0.5	1.0	0.0
(wd, wd)	0	0.3	2.0	3.8	4.0	5.0
$f_{\rm bin}$	0.5	0.408	0.405	0.379	0.362	0.449

The two 800-Myr-old luminosity functions are taken from the stars within the projected half-mass radius and stars farther away. The outer luminosity function (dashes) fits better to the bright stars, while the inner luminosity function fits better to the dimmer stars. Again we can argue that omitting the brightest stars from the sample provides a better fit to the observations, in which case the luminosity function of the inner half of the cluster provides a better comparison.

4.3 The Hyades

Fig. 18 compares the M_I-band luminosity functions for the stars and binaries of several models, at birth (dotted line) and at 600 Myr (other lines), with the observed luminosity function the Hyades (Reid & Hawley 1999). Reid & Hawley observed the entire cluster, and their luminosity function reportedly extends down to the hydrogen-burning limit. The $W_0 = 4$ data for the

Table 8. Stellar types from population synthesis study of 5×10^5 binaries. The numbers of binaries is renormalized to 1024 because this is the number of primordial binaries in each of our dynamical calculations. The evolution of population of 1024 single stars was presented in Table 2. Note that the dynamical models were performed with 1024 primordial binaries and 1024 single stars. We added the extra class of binaries which includes a neutron star or a black hole (indicated with remnant: rn), such binaries are omitted in the dynamical models due their small number.

time [Myr]:	0	100	200	400	600	800
ms	0	0.81	0.56	0.40	0.35	0.32
gs	0	0.43	0.52	0.78	1.12	1.14
wd	0	0.89	2.01	3.66	5.11	6.70
rn	0	4.52	4.52	4.53	4.53	4.53
(ms, ms)	1024	1009	1000	988.4	979.6	972.6
[ms, ms]	0	5.58	7.12	7.79	7.73	7.60
(ms, gs)	0	2.00	3.25	4.79	5.16	4.78
(ms, wd)	0	2.35	4.89	9.22	13.00	16.51
(ms, rn)	0	0.11	0.08	0.05	0.04	0.04
(gs, gs)	0	0.14	0.23	0.27	0.28	0.22
(gs, wd)	0	0.28	0.80	1.36	1.63	1.67
(gs, rn)	0	0.01	0.01	0.01	0.00	0.00
(wd, wd)	0	0.55	2.08	4.85	7.24	9.58
(wd, rn)	0	0.32	0.35	0.37	0.38	0.38
(rn, rn)	0	0.13	0.13	0.13	0.13	0.13

Table 9. Relative numbers of stars and binaries in the dynamical models, as fractions of the numbers found in the non-dynamical population synthesis studies. The normalization is such that the dynamical and non-dynamical calculations contain equal numbers of single main-sequence stars and main-sequence binaries. Numbers greater than 1 indicate excesses of those stellar type in the dynamical calculation; numbers less than 1 represent depletion.

	Normalized data for the W6 models					
time [Myr]:	0	100	200	400	600	800
ms	1	1	1	1	1	1
(ms, ms)	1	1	1	1	1	1
gs	0	1.1	0.7	0.9	1.0	1.5
wd	0	0.6	1.5	1.2	1.1	1.3
[ms, ms)	0	1.0	0.7	0.6	0.6	0.5
(ms, gs)	0	0.3	1.1	0.5	1.2	1.2
(ms, wd)	0	0.6	0.7	0.9	1.0	1.2
(wd, wd)	0	0.0	0.8	1.1	1.2	1.7
	Normalized data for the W4 models					
time [Myr]:	0	100	200	400	600	800
(ms, ms)	1	1	1	1	1	1
ms	1	1	1	1	1	1
gs	0	0.9	1.0	1.4	2.5	7.6
wd	0	0.5	1.2	1.3	1.8	4.7
[ms, ms)	0	1.3	0.9	0.7	0.7	0.7
(ms, gs)	0	0.5	1.2	0.5	1.3	3.1
(ms, wd)	0	1.1	0.7	0.5	1.2	1.8
(wd, wd)	0	0.7	1.2	1.3	1.5	2.6

entire cluster (solid) and the $W_0 = 6$ model for the stars within the half-mass radius (dash-3dot) do not fit as well as the data for model $W_0 = 4$ for stars within the inner half-mass radius (dashes). Our models W6 are somewhat farther from the Galactic Centre than the Hyades, which would tend to suppress mass segregation somewhat by increasing the cluster relaxation time. The $W_0 = 4$ models do exactly the opposite. It is not clear whether the overabundance of stars with $M_I \lesssim 9$ mag in the observed cluster can be compensated by some primordial mass segregation in the

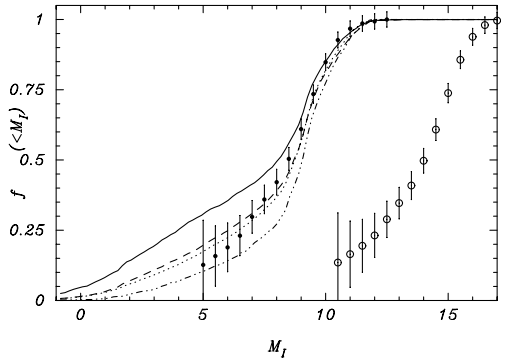

Figure 16. Cumulative luminosity function in M_I magnitudes. The open circles (○) with (Poissonian) error bars show the apparent luminosity function for the Pleiades (Hambly & Jameson 1991). The corrected absolute luminosity function, assuming a distance modulus $m - M = 5.5$ (Gatewood et al. 1990) is indicated by filled circles (●). Both luminosity functions are corrected for the 150 stars brighter than $m_I = 10.5$ (Pinfield et al. 1998). The dotted line is the initial luminosity function for all stars in the models (assuming that binaries are unresolved). The solid and dashed lines show the luminosity function for all models at $t = 100$ Myr within a projected (on to the y–z plane) 25 per cent Lagrangian and the half-mass radius of the cluster. The 3dot-dashed line give the luminosity function for the cluster stars in the outer 90 per cent Lagrangian radius.

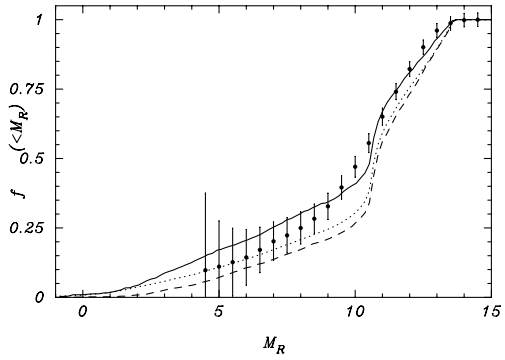

Figure 17. Cumulative luminosity function (M_R magnitude) of the Praesepe cluster. The filled circles with error bars give the observed luminosity function within the half-mass radius (Hambly at al. 1995a,b), to which 170 stars with $M_R < 4.5$ were added. The model W6 luminosity function for all stars at zero age is shown as a dotted line. The solid and dashed lines give the luminosity functions for models W6 at 800 Myr within and outside the projected (on to the y–z plane) half-mass radii.

model calculations, as the cluster is much older than an initial relaxation time. The degree of mass segregation can, however, be explained if Hyades was born with a somewhat smaller initial relaxation time, i.e., less massive and smaller in size. On the other hand, the mass of the cluster may initially not have been too small, otherwise the cluster would have dissolved in the tidal field of the Galaxy long ago.

Oort (1979) compared observations of Hyades with Aarseth's (1973, 1975) N-body calculations, and concluded that the outer 4 pc of the Hyades cluster are more strongly flattened, with $\epsilon \simeq 0.5$, than the N-body models implied. The orientation of the Hyades in the Galaxy relative to the position of the Sun then implies that the intrinsic flattening is even greater. Our calculations do not support Oort's conclusion, and a flattening of $\epsilon = 0.5$ is quite consistent with our N-body models. The reason for the discrepancy between our results and the conclusion of Oort is

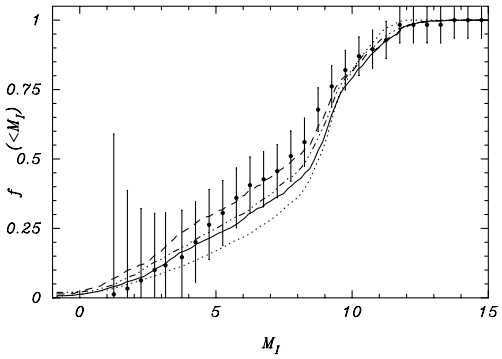

Figure 18. Cumulative M_I-magnitude luminosity function (filled circles with error bars) of the Hyades star cluster (Reid & Hawley 1999). The dotted line is the initial luminosity function for all stars in the model calculations. The solid and dashed lines give the luminosity function for model W4 at an age of 600 Mears for stars within the projected (on to the y–z plane) tidal radius (solid) and within the half-mass radius (dashes). The 3dot-dashed line gives the same data as the dashed line, but for model W6.

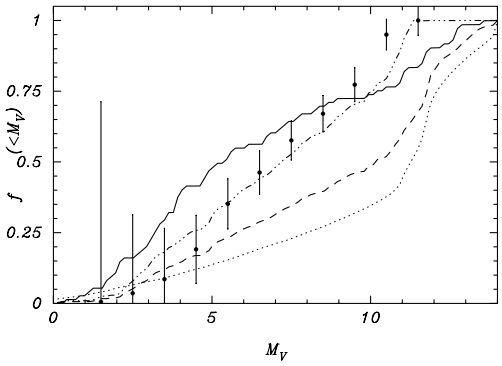

Figure 19. The filled circles with error bars show the observed cumulative luminosity function, corrected for field stars, of the star cluster NGC 3680 (Hawley et al. 1999). The dotted line gives the initial luminosity function for all models, and all other lines show luminosity functions at 1400 Myr. The solid and dashed lines give the luminosity function for all stars within the half-mass radius of model W4 and W6, respectively. The 3dot-dashed line shows only the stars with $M_V < 11.5$ from the dashed line (within the half-mass radius of model W6 at 1400 Myr).

based on Aarseth's models, which were computed with a very small number of stars. The flattening of the cluster in the tidal field of the Galaxy, however, becomes more apparent towards the clusters' tidal radius which has smallest stellar density. Calculations which are performed with a limited number of stars $\lesssim$500 will hardly show the flattening in the tidal field.

4.4 NGC 3680

Fig. 19 compares the observed M_V-band luminosity function of the old open cluster NGC 3680 with our model luminosity functions. The observed luminosity function is poorly reproduced by our cluster models. However, if we remove the least luminous stars (those with $V > 11.5$), the 1.4-Gyr model fits the observed luminosity function fairly well. The imposed lower limit is rather arbitrary; it suggests that the observations might not properly correct for the faintest stars, or that they may simply be absent from the data. Mass segregation generally causes the lightest stars to escape from the cluster which, in time, leads to an over-abundance of massive stars. The observed clusters, however, seem to have too few high-mass stars and also too few low-mass stars, which is hard to understand from a dynamical point of view. We therefore argue that in this case the lack of low-mass stars is caused by observational selection effects.

5 COMPARISON WITH OTHER WORK

Table 10 lists the initial conditions of previously reported results and compares the evaporation times with our own model calculations. We discuss each model in turn.

Terlevich (1987) performed direct N-body calculations with up to 1000 stars, including a power-law stellar mass function, mass-loss from single-star evolution, and the tidal field of the Galaxy. The implementation of the Galactic tidal field and the evolution of single stars were similar to those presented in this paper. Her model XII had initial conditions the closest to our own, although some significant differences exist. Terlevich's models started with spherical distribution of stars with density proportional to $1r^2$, virial radius 2 pc (half-mass radius of about 1.6 pc), and located at a distance of 10 kpc from the Galactic Centre. Her model XII initially consisted of 1000 stars drawn from a Salpeter mass function, with a mean mass of 0.5 $M_\odot$. The initial virial ratio, however, was $Q \equiv E_{\rm kin}/|E_{\rm pot}| = 0.25$, less than the equilibrium value of 0.5. This makes it hard to make a direct comparison with our models, which started in virial equilibrium. These cool initial conditions makes a comparison at the half-mass radius meaningless, but we can use the conditions at the tidal radius. The relaxation time at the tidal radius for our models W4 and W6 are about 0.8 and 2.2 Gyr, respectively, whereas Terlevich's model XII has a relaxation time at the tidal radius of about 1.5 Gyr. The half-life of model XII was 770 Myr. The run was terminated at 1 Gyr, by which time about 70 per cent of the mass had been lost. We estimate that the cluster would have dissolved in about 1.4 Gyr.

The lifetimes of our W4 and W6 models are 1.2 and 1.6 Gyr, respectively. The estimate for the lifetime of Terlevich's model XII is then reconcilable with that of our models, as we would expect that a model with a relaxation time of 1.5 Gyr [$\equiv 0.5 \times (0.8 + 2.2)$] at the tidal radius would live roughly 1.4 Gyr [$\equiv 0.5 \times (1.2 + 1.6)$].

Terlevich's model XII evolved through a phase of core collapse, which was aided by the absence of stars with masses greater than 10 $M_\odot$. By the time the turn-off mass has dropped below 10 $M_\odot$ (after about 22 Myr) our W6 models have lost between 4 and 9 per cent of their mass due to stellar evolution alone. The loss of even such a small mass fraction may have dramatic consequences for the further evolution of the stellar system, as this mass is lost from the most massive stars, which reside deep inside the cluster potential well. The shorter lifetime of clusters with large populations of massive stars is demonstrated by Terlevich's model XV, where the initial mean mass was 7.4 $M_\odot$ and the cluster did indeed dissolve much more rapidly.

The Galactic tidal field produced a similar flattening effect in Terlevich's clusters as in our own (compare her fig. 7 with our Fig. 12).

The simulations reported by McMillan & Hut (1994) included up to 2048 equal-mass stars, including up to 20 per cent rather soft primordial binaries, and incorporated the Galactic tidal field, modelled as the field of a distant point mass. However, they

Table 10. Overview of the model features, initial conditions and lifetimes of our model calculations and those reported by other workers. The Galactic tidal field may be modelled as that of a self-consistent disc (Disc) or a point mass (PM); initial density profiles are an anisotropic King model (AKing), an Isothermal sphere (Iso), or a Plummer sphere (Plummer) the latter two with a cut-off. Stellar and binary evolution are indicated by + (included) or − (for neglected). Note: Terlevich and de la Fuente Marcos work in terms of the initial virial radius, which is typically about 20 per cent bigger than the half-mass radius. Initially, model XII of Terlevich is not in virial equilibrium, and therefore we do not provide the initial half-mass relaxation time.

	Galaxy model	Density profile	Stellar evolution	Binary evolution	N	$\langle m \rangle$ [$M_\odot$]	$f_{\rm bin}$	$r_{\rm tide}$ [pc]	$r_{\rm hm}$ [pc]	$t_{\rm rlx}$ [Myr]	$t_{\rm end}$ [Myr]	$t_{\rm end}/t_{\rm rix}$
W4	Disc	AKing	+	+	3072	0.56	50	6.3	2.14	109	1200	11.0
W6	Disc	AKing	+	+	3072	0.54	50	12.1	2.00	102	∼1600	15.7
Terlevich	Disc	Iso	+	−	1000	0.50	0	12.1	1.70	–	∼1400	–
McMillan & Hut	PM	Plummer	−	−	2048	1	10	16.5	2.06	86	2500	29.0
Kroupa	PM	Plummer	+	−	400	0.32	100	6.5	2.53	77	693	9.0
de la Fuente Marcos	Disc	Iso	+	−	750	0.60	33	9.9	2.47	67	1061	15.8

excluded stellar evolution and hence any possibility of stellar mass-loss. In the absence of a physical time-scale associated with stellar evolution, they presented their results in units of the initial half-mass relaxation time. Our W6 models have half-lives of about 6 initial relaxation times, much shorter than the ∼29 initial relaxation times for the most comparable McMillan & Hut models. Also, as discussed previously, all the McMillan & Hut models experienced core collapse, which is absent in our simulations.

The main reasons for these differences are the effects of stellar mass-loss and the presence of a stellar mass function in the present studies. In our models, core collapse is arrested by a combination of effects, such as mass-loss binary activity and a large range in stellar masses. In addition, the McMillan & Hut models all started off well inside their tidal radii, significantly increasing their lifetimes.

In a continuing effort to understand the evolution of young open star clusters, Kroupa (1995a,b,c) performed N-body calculations with up to 400 stars, all of them members of primordial binaries. He adopted a distribution in orbital separation flat in $\log a$, but selected a between ∼360 and $\sim 3.6 \times 10^5\,R_\odot$; the binaries in his calculations were thus on average much wider than in our calculations. His models included the Galactic tidal field and stellar mass-loss, but neglected binary evolution.

Kroupa's model with the highest initial relaxation time started from a Plummer sphere with a half-mass radius of 2.5 pc and a crossing time of ∼20 Myr. It dissolved in about 700 Myr. Scaled to the initial relaxation time, this is somewhat faster than our W4 models. The main reasons for this more rapid evaporation are probably the shallower initial density profile in his models and the cluster's smaller distance from the Galactic Centre.

We compare the binary and triple properties of our models with those of McMillan & Hut and Kroupa in more detail in Paper V.

De la Fuente Marcos (1997) studied the effect of the initial mass function on the dynamical evolution of open star clusters, including both stellar mass-loss and the tidal field of the Galaxy. His calculations were limited to 750 stars and included 33 per cent rather wide primordial binaries, all with a mass ratio of 0.5, in which (binary) evolutionary effects were neglected. His model XX used Scalo's (1986) mass function and had an initial virial radius of 2.47 pc. The initial relaxation time for this model was about 67 Myr; the crossing time was 7.5 Myr. This model dissolved in about 1 Gyr, slightly faster than our models. However, scaled to the initial relaxation time, this result is consistent with the dissolution time of our W6 models (see Table 10).

6 SUMMARY AND DISCUSSION

The aim of our simulations is to study the evolution of open star clusters such as the Pleiades, Praesepe and the Hyades. These clusters differ significantly in age, but have comparable physical characteristics, stellar membership, total magnitude and internal velocity dispersions. Our N-body calculations incorporate, in a fully self-consistent fashion, mass-loss from single stars, binary evolution, dynamical encounters among single stars and binaries and the effect of the Galactic tidal field.

We have compared the luminosity functions, isochrones and projected luminosity profiles of our models with observations. For some clusters, it is hard to find a good match between model and observed luminosity functions. Mass segregation and observational limitations significantly reduce our ability to find a match, and restrict our understanding of the differences we see. However, we find that for models for which we compared the luminosity functions with Praesepe and the Hyades, the observations show a somewhat flatter luminosity function than is seen in the models. We conclude that these clusters may have been born somewhat mass segregated. Alternatively, these clusters may have started out somewhat more massive than assumed here, but with a shallower density profile. The selective evaporation of lower mass stars then results in a 'dynamically old' appearance (see also Takahashi & Portegies Zwart 2000).

The global luminosity function of Praesepe and its degree of mass segregation suggest an age greater than 800 Myr, which is at the high end of the observed range. The luminosity function of NGC 2287 is consistent with the observed age of 150–200 Myr. Our age estimates for the Pleiades and Hyades, based on the structure and dynamical state of these clusters, are consistent with ages derived from isochrone fitting.

6.1 Mass segregation

The first effects of mass segregation in our models are discernible in the cluster core after only a few million years, a small fraction of an initial half-mass relaxation time. After about a relaxation time, mass segregation becomes measurable in the cluster outskirts. The luminosity function of the inner parts of the cluster provides a useful tool for studying mass segregation, although one has to select regions which are well separated in radius in order to make the effect visible. As expected, giants and binary stars are most strongly affected by mass segregation, and it is easiest to identify the effect by comparing the radial distribution of giants with that of the lower mass main-sequence stars.

One important effect of mass segregation is that older clusters

become rich in white dwarfs and giants relative to the Galactic field. These stars may be single or members of binary systems. The main reason for the overabundance of giants and white dwarfs in clusters is the depletion of low-mass main-sequence stars by evaporation. This flattening of the mass function due to mass segregation has also been studied by Takahashi & Portegies Zwart (2000) for more massive clusters. They also find that clusters which are close to disruption are rich in compact objects and giant stars.

The W4 models have shallower initial potentials, lie closer to the Galactic Centre, and are more strongly affected by mass segregation because of their more rapid evaporation. We suggest that the best place to look for evidence of mass segregation is in star clusters with larger half-light radii, which have shallower potentials. Since mass segregation manifests itself more clearly in dynamically evolved systems, it is also better to look at older clusters. A relatively old cluster (age $\gtrsim$500 Myr) with a relatively small mass ($M_{\rm tot} \lesssim 500\,{\rm M}_\odot$) would be ideal.

6.2 Age estimates

The 'dynamical ages'[2] of our model clusters are often somewhat different from the ages determined by isochrone fitting. The instantaneous relaxation time is a poor estimator of a cluster's dynamical age. The cores of star clusters lose their memory of the initial relaxation time within a few million years, well within an initial half-mass relaxation time, but the time-scale for global cluster amnesia to set in is far greater than the initial relaxation time. The half-mass relaxation time tends to increase by a factor of 2 or 3, reaching a maximum near the cluster's half-life and decreasing thereafter. The increase is caused by the internal heating of the cluster; the decrease mainly by loss of stars.

6.3 Escaping stars

Stars tend to escape in the direction of the L_1 and L_2 Lagrange points of the Galaxy–cluster system. The velocities of the stars at these points are highly anisotropic and, as expected, pointing mostly radially away from the cluster centre. The velocities of the escaping stars are comparable to the cluster velocity dispersion; very few stars are ejected with high velocities following a strong dynamical encounter.

Neutron stars are ejected isotropically and with much higher velocities, owing to the asymmetric kicks they receive during the supernovae that create them. Binaries containing the progenitors of neutron stars are generally disrupted by the first supernova explosion; in all the calculations presented in this paper, only one binary survived the first supernova. However, the existence of that single binary does suggest that it may be possible to form X-ray binaries in open clusters. Such binaries are only expected to exist in star clusters which are younger than $\sim$45 Myr (the turn-off age of a 7-$M_\odot$ star), because mass-loss and the velocity kick imparted to the binary causes it to escape (see Paper V).

Black holes are more easily retained by the cluster, but are very rare due to their high progenitor mass and the steepness of the Scalo initial mass function.

6.4 Tidal flattening

The tidal field of the Galaxy flattens the cluster significantly in the z direction, and to a lesser extent along the y-axis. A cluster which is spherical at birth develops this flattening in its outer regions within a few crossing times; the inner parts remain fairly spherical. All our models show this flattening, but its observability from Earth depends on the orientation of the cluster in the Galactic plane.

Ellipticities reported for the Pleiades ($\epsilon \sim 0.3$; van Leeuwen et al. 1986) and Hyades ($\epsilon \sim 0.5$ in the outer regions; Oort 1979) are consistent with our model calculations. We inspected the spatial structures of NGC 2287, NGC 2516 and NGC 3680. The first two do not show significant flattening (NGC 2287 has $\epsilon \sim 0.05$, and NGC 2516 has $\epsilon \sim 0.14$), but these data contain only stars from the innermost 3 pc, which are least affected by the Galactic tidal field. NGC 3680 appears more square than elliptical. This may be caused by the small field of view of the telescope, which could cause a star cluster to take on the shape of the CCD frame.

The flattening in our models persists during mass segregation, in the sense that the mass-segregated Lagrangian radii are ellipsoids. Projection of the cluster on to the background may therefore decrease the observed mass segregation.

6.5 Core collapse

Our models experience rather shallow core collapse during their early evolution, followed by a more or less homologous expansion. The expansion is most likely driven by a combination of effects, among which stellar mass-loss and binary heating; dynamical models without stellar mass-loss, but which include a tidal field and primordial binaries, do show core collapse (McMillan & Hut 1994). Once the cluster has lost a considerable fraction of its stars, the system shrinks again. The remnant with a few remaining stars may become quite compact before it dissolves, but we find no evidence for late core collapse before complete disruption.

6.6 Giants and white dwarfs in open clusters

A cluster's single-star population is not noticeably affected by cluster dynamics until the age of the system exceeds $\sim$2 initial half-mass relaxation times. However, the binary populations are measurably influenced by dynamics even at early times (see Paper V). At later times ($t > 400$ Myr), our model clusters tend to become rich in giants and white dwarfs. Small-number statistics on the giants limit the degree to which we can quantify this statement, but the population of single white dwarfs in our models increased by factors of 1.3 to 4.7 (for models W6 and W4, respectively) relative to what one would expect for a non-dynamically evolving population of single stars and binaries.

Table 1 presents an overview of the numbers of white dwarfs observed in the clusters studied in this paper. Explaining the number of white dwarfs in the Hyades is a long-standing problem, starting with discussions in the mid-1970s by Tinsley (1974) and van den Heuvel (1975), and continuing into the 1990s (Eggen 1993; Weidemann 1993). All these papers conclude that the observed number of white dwarfs is too small, by about a factor of 3, for the inferred cluster mass and age. The three leading explanations were: (1) the upper mass limit for the production of white dwarfs may be as low as $\sim 4\,{\rm M}_\odot$ (Tinsley 1974), white dwarfs are born with a velocity kick as neutron stars do (Weidemann et al. 1992), and (3) mass segregation selectively ejects white dwarfs (van den Heuvel 1975). By studying the white dwarfs in NGC 2516, Koester & Reimers (1996) firmly conclude

[2] We define the dynamical age of a cluster as its lifetime expressed in units of the initial relaxation time.

that stars up to $8\,M_\odot$ can form white dwarfs, removing the first solution to this conundrum. However, our calculations are inconsistent with the idea that white dwarfs are preferentially ejected from star clusters by a dynamical process. On the contrary, the white dwarfs in our simulations are more easily retained than main-sequence stars of the same mass, causing the older clusters to become relatively white-dwarf-*rich* for their mass.

We can study this problem further by comparing the ratio of the number of white dwarfs to the number of giants: $f_{\frac{\rm wd}{\rm gs}} \equiv N_{\rm wd}/N_{\rm gs}$. For the first five open clusters in Table 1 this fraction ranges from $f_{\frac{\rm wd}{\rm gs}} = 1$ for NGC 2516 and the Pleiades to $f_{\frac{\rm wd}{\rm gs}} = 2.5$ for the Hyades. For an evolving population of single stars without dynamics (see Table 2), we find that the ratio ranges from 1.1 at 100 Myr (the age of NGC 2516) to 4.2 at 600 Myr (comparable to the age of Hyades).

Binary evolution complicates the comparison due to an obvious selection effect – the giants can probably all be seen, but white dwarfs are easily hidden near a main-sequence or giant companion. We obtain estimates for $f_{\frac{\rm wd}{\rm gs}}$ in a field population with 50 per cent primordial binaries by combining the single stars from Table 2 with the binaries from Table 8. We calculate an upper limit to $f_{\frac{\rm wd}{\rm gs}}$ by accounting for all white dwarfs [counting (wd, wd) binaries as two objects and including (ms, wd) and (gs, wd) binaries]. A lower limit is obtained by counting (wd, wd) binaries as one object and excluding white-dwarf binaries containing a main-sequence or giant companion. For the field (no dynamics) population, we find $f_{\frac{\rm wd}{\rm gs}} = 0.80$–$1.3$ at 100 Myr, and $f_{\frac{\rm wd}{\rm gs}} = 2.6$–$4.1$ at 600 Myr. Combining models W4 (Table 7) and W6 (Table 6), we obtain $f_{\frac{\rm wd}{\rm gs}} = 1.2$–$1.7$ at 100 Myr and $f_{\frac{\rm wd}{\rm gs}} = 3.2$–$4.0$ at 600 Myr.

The observed value of $f_{\frac{\rm wd}{\rm gs}} \sim 1$ at around 100 Myr seems somewhat low, but probably not inconsistent with our models. However, the value of $f_{\frac{\rm wd}{\rm gs}} \sim 2.5$ of the Hyades cluster (at about 600 Myr) is smaller than our models predict, suggesting that a considerable fraction of the white dwarfs are hidden in binaries.

The value of the fraction $f_{\frac{\rm wd}{\rm gs}}$ does not seem to pose a serious problem to understand any of the clusters discussed here, being less than a factor of 2 too small. However, according to the evolution of the field stars and binaries (combining Tables 2 and 8), at an age of 600 Myr we expect a total of about 15 giants and 60 white dwarfs. The comparable models W4 and W6 contain, respectively, 13 and 12 giants, and 48 and 55 white dwarfs at that age. Model W6 has lost about 40 per cent of its mass and model W4 about 60 per cent, yet the numbers of giants and white dwarfs have decreased by only 4–20 per cent. Averaging over time, we find a decrease in the number of giants and white dwarfs of about 2 per cent per 100 Myr. Apparently, the dynamical evolution of these clusters has little effect on the number of giants and white dwarfs. (In fact, this was assumed by von Hippel 1998 in estimating the mass fractions of white dwarfs in open clusters.) Number counts of giants and/or white dwarfs may therefore provide a reasonable estimate of a cluster's initial mass.

For a 50/50 mixture of single stars and binaries, meaning that 2/3 of the stars are binary components, the mean mass of a star is $\langle m\rangle = 0.46$ at $t = 100$ Myr, 0.41 at 600 Myr, and almost constant ($\langle m\rangle \sim 0.40$) thereafter. We use the numbers of giants to estimate the initial masses of the star clusters in Table 1, because the giants are least plagued by selection effects (although their small numbers significantly limit the accuracy of our estimates). The number of giants per 1k stars is 2.8 at 100 Myr (see Tables 2 and 8), and rises rapidly to about 6.5 at 600 Myr, after which the specific number of giants remains roughly constant. For an open cluster older than ~400 Myr, we thus estimate its initial mass via

$$M_0 = 65\,M_\odot N_{\rm gs}\left(1 + \frac{0.02t}{[100\,{\rm Myr}]}\right). \quad (1)$$

For younger clusters, the factor 65 ($= 1024 \times 0.41/6.5$) is larger (170 at 100 Myr and ~100 at 200 Myr).

We apply this method to the clusters from Table 1 with more than five giants and obtain the following birth masses: $830\,M_\odot$ for NGC 2287, $3100\,M_\odot$ for NGC 2660, and $1400\,M_\odot$ for NGC 3680. These mass estimates seem reasonable. For NGC 2534, Praesepe and the Hyades, the mass estimates are 690, 370 and $290\,M_\odot$, respectively, considerably smaller than the observed masses of these clusters (see Table 1).

The initial mass estimate for these clusters increases proportional to the number of giants. The ratio $f_{\frac{\rm wd}{\rm gs}}$ for these cluster does not pose a serious problem and therefore, instead of too few white dwarfs, Hyades seems to have too few giants. While white dwarfs can be hidden easily in binaries, giants are not so easy to hide. One way to decrease the number of giants is by binary activity. The number of giants can be decreased when subgiants are stripped in a phase of mass transfer before they reach the horizontal branch, where they spend most of their time. In order to reduce the number of giants in this fashion, we require a large fraction of binaries to be born with short orbital periods ($\lesssim$100 d). Alternatively, the giant lifetimes adopted in our models may be too long.

6.7 Notes on individual clusters

NGC 2516 deserves much more study, as its dynamical parameters (total mass, half-mass and core radii) are poorly known.

The Pleiades cluster has been quite thoroughly studied in searches for brown dwarfs and planets. Its mass function fits well with the luminosity function from our models, with the exception that our models contain too many bright stars.

NGC 2287 is quite poorly studied, and with the quoted values for the tidal radius it has an extremely low mass for its age (see Table 1). The presence of eight giants suggests that its mass must have been comparable to that of NGC 2516.

Praesepe has been studied recently in great detail, and appears to fit well with our dynamical models. However, the cluster is rather shallow and may have been born somewhat more massive and less concentrated ($W_0 \lesssim 4$) than our models. This conclusion is based on the observed shallow density profile and the high degree of mass segregation. There is some excess of stars with $V \sim 9$–11, unexplained by our models. The observed cluster seems to be very deficient in giants. Based on the number of white dwarfs and the dynamical state of the cluster we would expect at least 20 giants in this cluster, whereas only five are known.

The Hyades cluster fits well with our models, indicating that it is possible to estimate the initial conditions for an observed star cluster rather accurately. The cluster does not appear to be deficient in white dwarfs if we compare them to the number of giants. However, if the mass of Hyades quoted in Table 1 is correct, the observed number of white dwarfs and giants seems too small by a factor of about 3.

NGC 3680 fits well with our W6 models expect for the luminosity function, which is deficient of low-mass stars. A possible solution may be that these stars were initially absent in the cluster or that the observations do not go deep enough to reveal the low-mass stars.

6.8 Comparison with other work

Our models evaporate on time-scales generally consistent with dissolution times reported in previous calculations. The models of Terlevich (1987) and de la Fuente Marcos (1997) compare well with the evaporation times of our models. Terlevich's models evolve somewhat more slowly due to the lack of massive stars and the rather cool initial conditions, which drive the cluster to core collapse and therefore extend its lifetime somewhat. The models of McMillan & Hut (1994) dissolve more slowly than ours. This discrepancy can be completely explained by the absence of stellar evolution mass-loss and binary evolution in their models, along with the small size of those models relative to the clusters' tidal radii in the Galactic potential.

The only real discrepancy is with the work of Kroupa (1995a), whose models dissolve somewhat more rapidly than ours. Possibly the small numbers of stars and the large fraction of rather soft binaries drives a more rapid evaporation than one might naively expect. The evaporation rate of star clusters is known to depend on the total number of stars (Heggie et al. 1997; Portegies Zwart et al. 1998). In Section 1 we argue that the presence of primordial binaries has little effect on the cluster lifetime. It is, however, not clear how this trend propagates in the scaling of cluster lifetimes with respect to the number of stars.

ACKNOWLEDGMENTS

We thank Anthony Brown, Douglas Heggie, Ken Janes, Gijs Nelemans, Koji Takahashi and Lev Yungelson for numerous discussions. This work was supported by NASA through Hubble Fellowship grant HF-01112.01-98A awarded (to SPZ) by the Space Telescope Science Institute, which is operated by the Association of Universities for Research in Astronomy, Inc., for NASA under contract NAS 5-26555, by ATP grant NAG5-6964 (to SLWM) and by Research for the Future Program of Japan Society for the Promotion of Science (JSPS-RFTP97P01102). SFPZ is grateful to Drexel University, Tokyo University and the University of Amsterdam (under Spinoza grant 0-08 to Edward P. J. van den Heuvel) for their hospitality. Special thanks goes to the University of Tokyo for providing time on their GRAPE-4 system.

REFERENCES

Aarseth S. J., 1973, Vistas Astron., 15, 13
Aarseth S. J., 1975, in Hayly A., ed., Proc. IAU Symp. 69, Dynamics of Stellar Systems, p. 57
Aarseth S. J., 1999, PASP, 111, 1333
Aarseth S. J., Heggie D. C., 1998, MNRAS, 297, 794
Aarseth S. J., Lecar M., 1975, ARA&A, 13, 1
Abt H. A., Levy S. G., 1972, ApJ, 172, 355
Andrievsky S. M., 1998, A&A, 334, 139
Anthony-Twarog B. J., 1984, AJ, 89, 267
Binney J., Tremaine S., 1987, Galactic Dynamics. Princeton Univ. Press, p. 111
Bondi H., Hoyle F., 1944, MNRAS, 104, 273
Bouvier J., Rigaut F., Nadeau D., 1997, A&A, 323, 139
Casertano S., Hut P., 1985, ApJ, 298, 80
Chernoff D. F., Weinberg M. D., 1990, ApJ, 351, 121
Cox A. N., 1954, ApJ, 119, 188
Dachs J., Kabus H., 1989, A&AS, 78, 25
Davies M., Benz W., Hills J., 1991, ApJ, 381, 449
de la Fuente Marcos R., 1997, A&A, 322, 764
Duquennoy A., Mayor M., 1991, A&A, 248, 485
Eggen O. J., 1993, AJ, 106, 642
Eggleton P. P., 1983, ApJ, 268, 368
Eggleton P. P., Tout C. A., Fitchett M. J., 1989, ApJ, 347, 998
Eggleton P. P., Fitchett M. J., Tout C. A., 1990, ApJ, 354, 387
Farouki R. T., Salpeter E. E., 1982, ApJ, 253, 512
Farouki R. T., Salpeter E. E., 1994, ApJ, 427, 676
Frandsen S., Dreyer P., Kjeldsen H., 1989, A&A, 215, 287
Fukushige T., Heggie D. C., 1995, MNRAS, 276, 206
Fukushige T., Heggie D. C., 2000, MNRAS, 318, 753
Gao B., Goodman J., Cohn H., Murphy B., 1991, ApJ, 370, 569
Gatewood G., Castelaz M., Han I., Persinger T., Stein J., Stephenson B., Tangren W., 1990, ApJ, 364, 114
Goodman J., Hut P., 1989, Nat, 339, 40
Hambly N. C., Jameson R. F., 1991, MNRAS, 249, 137
Hambly N. C., Steele I. A., Hawkins M. R. S., Jameson R. F., 1995a, A&AS, 109, 29
Hambly N. C., Steele I. A., Hawkins M. R. S., Jameson R. F., 1995b, MNRAS, 273, 505
Harris G. L. H., Fitzgerald M. P. V., Mehta S., Reed B. C., 1993, AJ, 106, 1533
Hartman J. W., 1997, A&A, 322, 127
Hartwick F. D. A., Hesser J. E., 1971, PASP, 83, 53
Hawley S. L., Tourtellot J. G., Reid I. N., 1999, AJ, 117, 1341
Heacutenon M., 1972, in Lecar M., ed., Proc. IAU Colloq. 10, Gravitational N-Body Problem. Dordrecht Reidel Publishing Company, p. 111
Heggie D. C., 1975, MNRAS, 173, 729
Heggie D. C., 1992, Nat, 359, 772
Heggie D. C., Ramamani N., 1995, MNRAS, 272, 317
Heggie D. C., Giersz M., Spurzem R., Takahashi K., 1997, in Andersen J., eds, Highlights of Astronomy Vol. 11. Kluwer, Dordrecht, p. 591
Henon M., 1972, A&A, 19, 480
Hjellming M. S., Webbink R. F., 1987, ApJ, 318, 794
Hodgkin S. T., Pinfield D. J., Jameson R. F., Steele I. A., Cossburn M. R., Hambly N. C., 1999, MNRAS, 310, 87
Hurley J. R., Pols O. R., Tout C. A., 2000, MNRAS, 315, 543
Hut P. et al., 1992, PASP, 104, 981
Ianna P. A., Adler D. S., Faudree E. F., 1987, AJ, 93, 347
Jones B. F., Stauffer J. R., 1991, AJ, 102, 1080
King I. R., 1966, AJ, 71, 64
Koester D., Reimers D., 1981, A&A, 99, L8
Koester D., Reimers D., 1996, A&A, 313, 810
Kroupa P., 1995a, MNRAS, 277, 1491
Kroupa P., 1995b, MNRAS, 277, 1507
Kroupa P., 1995c, MNRAS, 277, 1522
Lai D., Rasio F. A., Shapiro S. L., 1993, ApJ, 406, L63
Langer N., 1998, A&A, 329, 551
Livio M., Truran J. W., 1992, ApJ, 389, 695
Lombardi J. C. J., Rasio F. A., Shapiro S. L., 1995, ApJ, 445, L117
Lyngå G., 1987, Catalog of Open Cluster Data, Computer based catalogue available through the CDS. 5th edition, Vol. 4, Strasbourg, France and through NASA Data Center, Greenbelt, Maryland, USA, p. 121
Makino J., Aarseth S. J., 1992, PASJ, 44, 141
Makino J., Taiji M., Ebisuzaki T., Sugimoto D., 1997, ApJ, 480, 432
McMillan S. L. W., 1986, ApJ, 307, 126
McMillan S. L. W., Hut P., 1994, ApJ, 427, 793
McMillan S. L. W., Hut P., Makino J., 1990, ApJ, 362, 522
McMillan S. L. W., Hut P., Makino J., 1991a, ApJ, 372, 111
McMillan S. L. W., Hut P., Makino J., 1991b, in Janes K., eds, The Formation and Evolution of Star Clusters, ASP Conf. Ser., Vol. 13, 421
Mermilliod J. C., Mayor M., 1999, A&A, 352, 479
Mermilliod J. C., Weis E. W., Duquennoy A., Mayor M., 1990, A&A, 235, 114
Meylan G., Heggie D. C., 1997, A&AR, 8, 1
Mikkola S., Aarseth S. J., 1998, New Astronomy, 3, 309
Nelemans G., Verbunt F., Yungelson L. R., Portegies Zwart S. F., 2000, A&A, 360, 1011
Nomoto K., Kondo Y., 1991, ApJ, 367, L19

Nordström B., Andersen J., Andersen M. I., 1996, A&AS, 118, 407
Nordström B., Andersen J., Andersen M. I., 1997, A&A, 322, 460
Oort J., 1927, Bull. Astron. Inst. Neth., 3, 275
Oort J. H., 1979, A&A, 78, 312
Perryman M. A. C. et al., 1998, A&A, 331, 81
Peters P. C., 1964, Phys. Rev., 136, 1224
Pinfield D. J., Jameson R. F., Hodgkin S. T., 1998, MNRAS, 299, 955
Portegies Zwart S. F., 1996, in Milone E. F., Mermilliod J.-C., eds, ASP Conf. Ser. Vol. 90. Astron. Soc. Pac., San Francisco, p. 378
Portegies Zwart S. F., Verbunt F., 1996, A&A, 309, 179
Portegies Zwart S. F., Yungelson L. R., 1998, A&A, 332, 173
Portegies Zwart S. F., Hut P., McMillan S. L. W., Verbunt F., 1997a, A&A, 328, 134 (Paper I)
Portegies Zwart S. F., Hut P., Verbunt F., 1997b, A&A, 328, 130 (Paper II)
Portegies Zwart S. F., Hut P., Makino J., McMillan S. L. W., 1998, A&A, 337, 363
Portegies Zwart S. F., Makino J., McMillan S. L. W., Hut P., 1999, A&A, 348, 117 (Paper III)
Raboud D., Mermilliod J. C., 1998, A&A, 329, 101
Rappaport S., Joss P. C., Verbunt F., 1983, ApJ, 275, 713
Rasio F., Shapiro S., 1991, ApJ, 377, 559
Rasio F., Shapiro S., 1995, ApJ, 438, 887
Reid I. N., Hawley S. L., 1999, AJ, 117, 343
Rubenstein E. P., 1997, PASP, 109, 933
Ruffert M., Müller E., 1990, A&A, 238, 116
Sandrelli S., Bragaglia A., Tosi M., Marconi G., 1999, MNRAS, 309, 739
Scalo J. M., 1986, Fundam. Cosmic Phys., 11, 1
Smith H. J., 1992, ApJ, 398, 519
Spitzer L., 1987, Dynamical Evolution of Globular Clusters. Princeton Univ. Press, Princeton, NJ, p. 191
Takahashi K., Portegies Zwart S. F., 2000, ApJ, 535, 759
Terlevich E., 1987, MNRAS, 224, 193
Thorne K. S., Żytkow A. N., 1977, ApJ, 212, 832
Tinsley B. M., 1974, PASP, 86, 554
Tout C. A., Aarseth S. J., Pols O. R., 1997, MNRAS, 291, 732
van den Heuvel E. P. J., 1975, ApJ, 196, L121
van Leeuwen F., Alphenaar P., Brand J., 1986, A&AS, 65, 309
Verbung F., Hut P., 1987, in Hefand D. J., Huang J.-H., eds, Proc. IAU Symp. 125, The Origin and Evolution of Neutron Stars. Reidel, Dordrecht, p. 187
von Hippel T., 1998, AJ, 115, 1536
von Hoerner S., 1960, Z. Astrophys., 50, 184
von Hoerner S., 1963, Z. Astrophys., 57, 47
Webbink R. F., 1984, ApJ, 277, 355
Weidemann V., 1993, A&A, 275, 158
Weidemann V., Jordan S., Iben I. J., Casertano S., 1992, AJ, 104, 1876

APPENDIX A: TERMINOLOGY

Throughout the paper (and in future papers in this series) we will use consistent nomenclature. Some of these terms are rather confusing and have been used by different authors in the past with slightly different meanings. For clarity, we present here a short glossary of terms.

Binary fraction: Throughout this paper we define the binary fraction as

$$f_{\rm bin} = \frac{N_{\rm bin}}{N_{\rm sing} + N_{\rm bin}}. \tag{A1}$$

Here $N_{\rm sing}$ and $N_{\rm bin}$ are the number of single stars and binaries.

Cluster centre: The density centre of the cluster, as defined below. Alternative definitions may use the number density or the luminosity density, or the point where the density is greatest, and may include projection effects.

Collision: A collision occurs when the distance between two stars i and j becomes smaller than the sum of their effective radii: $d < d_{\rm coll}(r_i + r_j)$, with $d_{\rm coll} = 1$. The effective radii are determined from detailed fluid-dynamical calculations.

Core radius: The weighted average distance of all stars from the density centre. Casertano & Hut (1985) originally used a weighting proportional to the local density. However, in practice this definition is unsuitable for clusters with near-isothermal density profiles ($\rho \sim r^{-2}$). Following Aarseth (1986), we adopt the modified definition

$$r_{\rm core} \equiv \frac{\sum_i |r_i - r_j| {\rho_j^{(i)}}^2}{\sum_i {\rho_j^{(i)}}^2}, \tag{A2}$$

where ρ_j is given by equation (A6). Note that this definition of the core does not *necessarily* have any simple relation to the 'core radius' normally quoted by observers, nor to the 'dynamical' core radius $r_{\rm c} = \sqrt{3\langle v^2\rangle_{\rm c}/4\pi G\rho_{\rm c}}$, where $\rho_{\rm c}$ and $\langle v^2\rangle_{\rm c}$ are, respectively, the cluster's central density and velocity dispersion (Binney & Tremaine 1987).

Crossing time: The time taken by a star with velocity equal to the velocity dispersion v to cross the virial radius r of the stellar system $t_{\rm c} = r/v$, which for practical reasons is written as

$$t_{\rm c} \equiv \left(\frac{r_{\rm vir}^3}{GM}\right)^{1/2}. \tag{A3}$$

In more convenient units, we write the half-mass crossing time as

$$t_{\rm hm} = 57\left(\frac{[{\rm M}_\odot]}{M_{\rm tot}}\right)^{1/2}\left(\frac{r_{\rm hm}}{[{\rm pc}]}\right)^{3/2}[{\rm Myr}]. \tag{A4}$$

Density centre: The density weighted average of the positions of all stars (von Hoerner 1960, 1963):

$$\boldsymbol{r}_{\rm dens} \equiv \frac{\sum_i \boldsymbol{r}_i \rho_j^{(i)}}{\sum_i \rho_j^{(i)}}. \tag{A5}$$

In these expressions, $\rho_j^{(i)}$ is the density estimator of order j around the ith particle, with position vector $\boldsymbol{r}_i$. For any star i we define the local density within the volume V_j of the sphere containing the j nearest neighbours (i_1, i_2, …, i_j) of i as

$$\rho_j^{(i)} \equiv \frac{\sum_{k=1}^{j-1} m_{i_k}}{V_j}, \tag{A6}$$

where $V_j = \frac{4\pi}{3}|r_{i_j} - r_i|^3$, and the sum over masses excludes the masses of both stars i and i_j (see Casertano & Hut 1985). We take $j = 12$.

Escaper: A star which is not bound to the cluster, i.e., whose energy exceeds the energy at the cluster's Jacobi surface. An escaper may lie within the Jacobi surface.

Half-mass radius: The radius of the sphere, centred on the cluster density centre, that contains half of the total cluster mass (as defined in the text). It is not always clear which stars to include in determining this radius, as the cluster is generally flattened in the Galactic tidal field.

Hard binary: A binary whose binding energy exceeds the mean stellar energy in the cluster (Heggie 1975). A binary is hard if its semimajor axis is less than

$$a = \frac{GMm(M + m + m_3)}{(M + m)m_3 v^2}. \tag{A7}$$

Jacobi radius: The distance from the cluster centre to the L_1 and L_2 Lagrange points – the maximum distance from the cluster centre to the cluster Jacobi surface.

Jacobi surface: The cluster's 'Roche lobe' in the tidal field of the Galaxy. Consider a star moving with Jacobi integral $E_J \equiv \frac{1}{2}v^2 + \phi_{\rm eff}(\boldsymbol{r})$ in the rotating frame of reference in which our simulations are performed, where v is velocity, and the effective potential $\phi_{\rm eff}$ includes the cluster's self-gravity, the tidal field of the Galaxy, and the centrifugal force in the rotating frame. The *zero-velocity surface* for that value of E_J is defined by $v = 0$, so $\phi_{\rm eff}(\boldsymbol{r}) = E_J$ (Binney & Tremaine 1987). The Jacobi surface for the cluster is defined to be the last closed zero-velocity surface that contains the cluster – that is, the surface passing through the cluster's L_1 and L_2 Lagrange points. With the conventions adopted in kira, the Lagrange points are located along the x-axis, the cluster orbits in the x–y plane, and the Jacobi surface is elongated in the x-direction. The three coordinate axes intersect the Jacobi surface at distances $r_x = r_J$ (the Jacobi radius), r_y, and r_z from the cluster centre.

Member: A star (or multiple system) which is bound to the cluster. The energy of such a star is less than the energy at the cluster Jacobi surface. A member may lie outside the Jacobi surface.

Primary: The more massive of the two stars in a binary system. Denoted by M.

Relaxation time: We use Spitzer's (1987) definition of the half-mass relaxation time:

$$t_{\rm rlx} = \left(\frac{r_{\rm hm}^3}{GM}\right)^{1/2} \frac{N}{8\log\Lambda}. \tag{A8}$$

Here $\Lambda \simeq 0.4N$ is the Coulomb logarithm. (In the presence of a realistic mass function, $\Lambda \lesssim 0.1N$ may be more appropriate; Farouki & Salpeter 1982, 1994; Smith 1992; Fukushige & Heggie 2000.) In convenient units this may be written as

$$t_{\rm rlx} = 2.05\left(\frac{[{\rm M}_\odot]}{M_{\rm tot}}\right)^{1/2}\left(\frac{r_{\rm hm}}{[{\rm pc}]}\right)^{3/2}\frac{N}{\log\Lambda}[{\rm Myr}]. \tag{A9}$$

Note that 'N' here is the number of bound objects (a binary is a single object) in the star cluster, and is smaller than the total number of stars if the cluster contains binaries.

Secondary: The less massive of the two stars in a binary system. Denoted by m.

Tidal radius: Since clusters are somewhat elongated in the Galactic tidal field, the tidal 'radius' is not well defined. For definiteness, we take the tidal radius to be the Jacobi radius of the cluster. For a disc field described by Oort (1927) constants A and B, we have

$$r_{\rm tide}^3 = \frac{GM_{\rm tot}}{4A(A-B)}[{\rm pc}]. \tag{A10}$$

In the solar neighbourhood, $A = 15\,{\rm km\,s^{-1}\,kpc^{-1}}$, and $B = -12\,{\rm km\,s^{-1}\,kpc^{-1}}$.

Unperturbed binary: A binary for which the dimensionless perturbation due to its neighbours is less than some critical value (typically 10^{-6}). Dynamically, unperturbed binaries are treated in the point-mass approximation, as seen by the rest of the system. Only unperturbed binaries can be treated using the SeBa binary evolution module described in Appendix B. Perturbed binaries are treated as two single stars; mass transfer and tidal circularization are currently not handled in perturbed binaries.

Virial radius: A characteristic length-scale for the system, defined by

$$r_{\rm vir} = \frac{GM_{\rm tot}^2}{-2U}, \tag{A11}$$

where U is the total potential energy of the system (including the tidal potential). For an isolated equal-mass system, $r_{\rm vir}$ is the harmonic mean of the particle separations (Hénon 1972).

APPENDIX B: STARLAB

The simulations described in this series of papers are carried out within the 'Starlab' software environment, version 3.5. Starlab is a software package for simulating the evolution of dense stellar systems and analysing the resultant data. It consists of a collection of loosely coupled programs ('tools') linked at the level of the UNIX operating system. The tools share a common data structure and can be combined in arbitrarily complex ways to study the dynamics of star clusters and galactic nuclei. The main components of Starlab used in this work are kira, the N-body integrator, and SeBa, a stellar and binary evolution package. The Starlab system is described in detail in `http://www.manybody.org/`.

B1 Kira

The N-body integrator kira is the largest single program within Starlab. Its basic function is to take an input N-body system and evolve it forward for a specified period of time, producing snapshot and other diagnostic output at regular intervals. In addition to strictly dynamical evolution of stars and multiple stellar systems, kira also incorporates stellar and binary evolution (via the SeBa subpackage), and the possible influence of an external ('tidal') gravitational field. The program is designed to take advantage of the 'GRAPE-4' special-purpose processor (Makino et al. 1997), if available, although GRAPE is not required for its operation.

B1.1 The integrator

Particle motion is followed using a fourth-order, block-time-step (McMillan 1986) 'Hermite' predictor-corrector scheme (Makino & Aarseth 1992). Briefly, during a time-step δt, particle positions $\boldsymbol{x}$ and velocities $\boldsymbol{v}$ are first predicted using the known acceleration $\boldsymbol{a}$ and 'jerk' $\boldsymbol{j}$ (the time derivative of the acceleration):

$$\boldsymbol{x}_{\rm p} = \boldsymbol{x} + \boldsymbol{v}\delta t + \tfrac{1}{2}\boldsymbol{a}\delta t^2 + \tfrac{1}{6}\boldsymbol{j}\delta t^3, \tag{B1}$$

$$\boldsymbol{v}_{\rm p} = \boldsymbol{v} + \boldsymbol{a}\delta t + \tfrac{1}{2}\boldsymbol{j}\delta t^2. \tag{B2}$$

The acceleration $\boldsymbol{a}_{\rm p}$ and jerk $\boldsymbol{j}_{\rm p}$ are then computed at the predicted time using $\boldsymbol{x}_{\rm p}$ and $\boldsymbol{v}_{\rm p}$, and the motion is corrected using the additional derivative information thereby obtained,

$$\boldsymbol{k} \equiv \tfrac{1}{2}\boldsymbol{a}''\delta t^2 = 2(\boldsymbol{a} - \boldsymbol{a}_{\rm p}) + \delta t(\boldsymbol{j} - \boldsymbol{j}_{\rm p}), \tag{B3}$$

$$\boldsymbol{l} \equiv \tfrac{1}{6}\boldsymbol{a}'''\delta t^3 = -3(\boldsymbol{a} - \boldsymbol{a}_{\rm p}) - \delta t(2\boldsymbol{j} + \boldsymbol{j}_{\rm p}), \tag{B4}$$

to obtain the corrected position and velocity:

$$\boldsymbol{x}_{\rm c} = \boldsymbol{x}_{\rm p} + \left(\frac{1}{20}\boldsymbol{l} + \frac{1}{12}\boldsymbol{k}\right)\delta t^2, \tag{B5}$$

$$\boldsymbol{v}_{\rm c} = \boldsymbol{v}_{\rm p} + \left(\tfrac{1}{4}\boldsymbol{l} + \tfrac{1}{3}\boldsymbol{k}\right)\delta t. \tag{B6}$$

A single integration step in thus proceeds as follows.

(i) Determine which stars are to be updated next. Each star has associated with it an individual time t, representing the time to which it was last advanced, and an individual time-step δt. The list of stars to be integrated consists of those with the least value of $t+\delta t$. Time-steps are constrained to be powers of 2, allowing 'blocks' of many stars to be advanced simultaneously.

(ii) Before the step is actually taken, check for

(a) termination of the run;
(b) escaper removal;
(c) system reinitialization;
(d) diagnostic ('log') output, which includes
– information on bulk parameters of the system: total mass, energy, momentum, anisotropy, etc.,
– technical information on CPU time, time-step distribution, etc.,
– detailed information on the cluster mass distribution: core properties, Lagrangian radii, etc.,
– stellar mass distribution and anisotropy by Lagrangian zone,
– luminosity profile, and mass and luminosity functions,
– cluster stellar content (by spectral type and luminosity class),
– detailed dynamical and physical data on all binary systems, and
(e) snapshot output, for restart and display.

(iii) Perform low-order prediction of all particles to the new time. This operation may be performed on the GRAPE, if present.

(iv) Recompute the acceleration and jerk on all stars in the current block (using the GRAPE, if available), and correct their positions and velocities for fourth-order accuracy.

(v) Check for and initiate unperturbed motion.

(vi) Check for collisions and mergers.

(vii) Check for tree reorganization (see below).

(viii) Check for and apply stellar and/or binary evolution (Section B.2), and correct the dynamics whenever necessary.

B1.2 Tree structure

An N-body system in Starlab is represented as a linked-list structure, in the form of a mainly 'flat' tree having individual stars as leaves. The tree is flat in the sense that single stars (i.e., stars that are not members of any multiple system) are all represented as top-level nodes, having the root node (the system centre of mass) as parent. Binary, triple, and more complex multiple systems are represented as binary trees below their top-level centre of mass nodes. The tree structure determines both how node dynamics is implemented and how the long-range gravitational force is computed.

Each parent node contains 'local' information about its dynamics – mass, position, velocity, etc. – relative to its parent node. The leaves contain additional information about stellar properties – effective radius, luminosity, temperature, etc. The parent node of a unperturbed binary also contains information on the binary parameters – semimajor axis, eccentricity, mean anomaly, etc. The motion of every node *relative to its parent node* is followed using the Hermite predictor-corrector scheme just described. The use of relative coordinates at every level ensures that high numerical precision is maintained at all times, even during very close encounters.

The tree evolves dynamically according to simple heuristic rules: particles that approach 'too close' to one another are combined into a centre of mass and binary node; when a node becomes 'too large', it is split into its binary components. These rules apply at all levels of the tree structure, allowing arbitrarily complex systems to be followed. In practice, the term 'too close' is taken to mean that two stars (1 and 2) approach within the 'close-encounter distance' $R_{\rm close} \sim r_{\rm vir}(m_1+m_2)/2M_{\rm tot}$, the impact parameter that would lead to a 90° deflection if both bodies moved at typical stellar speeds. 'Too large' means that a node's diameter exceeds $2.5R_{\rm close}$.

B1.3 Binaries

How the acceleration (and jerk) on a particle or node is computed depends on its location in the tree. Top-level nodes feel the force due to all other top-level nodes in the system. Forces are computed using direct summation over all other particles in the system; no tree or neighbour-list constructs are used. (This procedure is designed specifically to allow efficient computation of these forces using GRAPE hardware, if available.) Nearby binary and multiple systems are resolved into their components, as necessary.

The internal motion of a binary component is naturally decomposed into two parts: (1) the dominant contribution due to its companion, and (2) the perturbative influence of the rest of the system. This decomposition is applied recursively, at all levels in a multiple system. Since the perturbation drops off rapidly with distance from the binary centre of mass, usually only a few near neighbours are significant perturbers of even a moderately hard binary. These neighbours are most efficiently handled by maintaining lists of perturbers for each binary. Perturber lists are recomputed at time the centre of mass is integrated.

A further efficiency measure is the imposition of *unperturbed motion* for binaries whose perturbation falls below some specified value for all or part of an orbit. Unperturbed binaries may be followed analytically for many orbits as strictly two-body motion; they are also treated as point masses, from the point of view of their influence on other stars. The use of the unperturbed approximation near the periastron of eccentric orbits was a key element in our decision not to use complex regularization schemes for the computation of binary motion.

Because unperturbed binaries are followed in steps that are integer multiples of the orbit period, we can relax the perturbation threshold for unperturbed motion relative to that for a perturbed step (since most of the perturbative effects of nearby stars are periodic). Perturbed binaries are resolved into their components, both for purposes of determining their centre-of-mass motion and for determining their effect on other stars. Unperturbed treatments of multiple systems are also used, based on empirical studies of the stability of their internal motion. A hierarchical system is regarded as stable if (a) the external perturbation is less than some threshold value, and (b) each component is stable (or single), by the same criterion.

'Lightly perturbed' binaries, having external perturbations within a factor of $\sim$10 of the unperturbed threshold, are treated using a variant of the method described by Mikkola & Aarseth (1998), in which the internal motion of the binary is artificially slowed and the perturbation is increased by the same factor. Briefly, the result is that long-term secular trends in the binary orbital elements are properly reproduced, while periodic perturbative terms are amplified; the latter effect is suppressed by following the 'slow' motion over an integral number of orbits. Our 'slow' binary treatment differs from that of Aarseth mainly in that it is not coupled to a regularization scheme – it is applied directly

to the unregularized equations of motion. In addition, we apply pairwise corrections to forces between perturbers and the binary centre of mass in order to avoid spurious high derivatives caused by the mismatch between the (slowed) internal motion and the (normal) external interaction.

B1.4 Tidal field

The standard form of the external (tidal) potential is

$$\phi_{\rm ext} = \tfrac{1}{2}(\alpha_1 x^2 + \alpha_3 z^2). \tag{B7}$$

This expression includes contributions from both the Galactic tidal field and the centrifugal force in the cluster's rotating frame of reference. The Galactic Centre is assumed to lie along the negative x-axis, and the rotation vector $\boldsymbol{\Omega}$ is in the z-direction. (We assume motion in a circular orbit in the x-y plane around the Galactic Centre.) The equations of motion also include a Coriolis acceleration $\boldsymbol{a}_{\rm c} = -2\boldsymbol{\Omega}\times\boldsymbol{v}$. Tidal and Coriolis effects are applied to top-level nodes only, i.e., we neglect the tidal effect of the Galaxy on a binary's internal motion.

The values of α_1, α_3, and Ω depend on the details of the field being modelled. Some common examples are the following.

(i) *Point-mass field.* If the Galaxy is represented as a point mass $M_{\rm G}$ at distance $R_{\rm G}$, we have

$$\alpha_3 = -\frac{1}{3}\alpha_1 = \Omega^2 = \frac{GM_{\rm G}}{R_G^3}. \tag{B8}$$

(ii) *Isothermal field.* For motion in a 'halo' mass distribution modelled as an isothermal sphere ($\rho \sim r^{-2}$), with $M(<r) = M_{\rm G}(r/R_{\rm G})$, we have

$$\alpha_3 = -\frac{1}{2}\alpha_1 = \Omega^2 = \frac{GM_{\rm G}}{R_G^3}. \tag{B9}$$

(iii) *Disc field.* For motion in a disc described by local Oort constants A and B, with local density $\rho_{\rm D}$, we have

$$\alpha_1 = -4A(A-B), \tag{B10}$$

$$\alpha_3 = 4\pi G\rho_{\rm D} + 2(A^2 - B^2), \tag{B11}$$

$$\Omega = A - B. \tag{B12}$$

In the (fairly good) approximation that the gravitational potential of the cluster stars may be represented close to the Jacobi surface simply as $\phi_{\rm C}(r) \sim -GM_{\rm tot}/r$, where $M_{\rm tot}$ is the cluster mass, the Jacobi radius may straightforwardly be shown to be

$$r_{\rm J} \approx \left(\frac{-GM_{\rm tot}}{\alpha_1}\right)^{-1/3}. \tag{B13}$$

The ratio α_3/α_1 determines the shape of the Jacobi surface.

B1.5 Escaper removal

Stars are removed ('stripped') from the system when they exceed a specified distance from the cluster centre of mass (or density centre). For systems without an imposed Galactic tidal field, this stripping radius is arbitrary. For systems with a tidal field, the stripping radius is usually tied to the Jacobi radius of the cluster. For the runs described in this paper, stars were stripped when their distance from the cluster centre exceeded twice the instantaneous Jacobi radius.

B2 SeBa

The stellar and binary evolution package SeBa[3] is fully integrated into the kira integrator, although it can also be used as a stand-alone module for non-dynamical applications.

B2.1 Evolution of a single star

Stars are evolved via the time-dependent mass–radius relations for solar metallicities given by Eggleton et al. (1989, with corrections by Eggleton, Fitchett & Tout 1990 and Tout, Aarseth & Pols 1997).[4] These equations give the radius of a star as a function of time and the star's initial mass (on the ZAMS). Neither the mass of the stellar core nor the rate of mass-loss via a stellar wind are specified in this prescription. However, both quantities are important, both to binary evolution and to cluster dynamics. We include them using the prescriptions of Portegies Zwart & Verbunt (1996).

Stars are subdivided within SeBa into the following types:

planet Various types, such as gas giants, etc.; also includes moons.

brown dwarf Star with mass below the hydrogen-burning limit.

main sequence Core hydrogen burning star.

hypergiant Massive ($m > 25\,{\rm M}_\odot$) post-main-sequence star with enormous mass-loss rate in a stage of evolution prior to becoming a Wolf–Rayet star.

helium star Helium core of a stripped giant, the result of mass transfer in a binary. Subdivided into helium core, carbon core and helium giant.

Hertzsprung gap Rapid evolution from the terminal-age main sequence to the point when the hydrogen-depleted core exceeds the Schönberg–Chandrasekhar limit.

subgiant Hydrogen shell burning star.

horizontal branch Helium core burning star.

supergiant Double shell burning star.

Thorne–Żytkow Shell burning hydrogen envelope with neutron star core.

black hole Star with radius smaller than the event horizon. The result of evolution of massive ($m > 25\,{\rm M}_\odot$) star or collapsed neutron star.

neutron star Subdivided into radio pulsar, X-ray pulsar and inert neutron star ($m < 2\,{\rm M}_\odot$).

white dwarf Subdivided into helium dwarf, carbon dwarf and oxygen dwarf.

disintegrated Result of carbon detonation to Type Ia supernova.

Stellar-wind mass-loss is neglected for main-sequence stars with $m < 25\,{\rm M}_\odot$. Following Langer (1998), more massive stars lose mass with $\dot{m} \propto m^{2.5}$ before becoming a Wolf–Rayet star (see Paper III, for the implementation). These stars eventually collapse into black holes with mass $m_{\rm bh} = 0.35m_0 - 12\,{\rm M}_\odot$, where m_0 is the initial mass of the star. (For a star whose mass increases due to collisions or other processes, m_0 is the highest mass reached by the star. The black hole radius equals the Schwarzschild radius: $r = 2Gm/c^2$.)

[3] The name SeBa is taken from the ancient Egyptian word for 'to teach', 'the door to knowledge' or '(multiple) star'. The exact meaning depends on the hieroglyphic spelling.

[4] New equations which include metallicity dependence have recently been made available by Hurley, Pols & Tout (2000), and will be implemented in the next version of SeBa.

A star with a helium core mass between 2.2 and 5 $M_\odot$ becomes a neutron star. (These limits correspond to 8- and 25-$M_\odot$ ZAMS stars which evolve as isolated single stars.) At birth, a neutron star receives a velocity 'kick' in a random direction. The magnitude of the velocity kick is chosen randomly from the distribution proposed by Hartman (1997):

$$P(u)\,\mathrm{d}u = \frac{4}{\pi}\frac{\mathrm{d}u}{(1+u^2)^2}, \tag{B14}$$

with $u = v/\sigma$ and $\sigma = 600\,\mathrm{km\,s^{-1}}$.

A star with a core mass less than 2.2 $M_\odot$ sheds its envelope at the end of its evolution and becomes a white dwarf. The mass of the white dwarf equals the core mass of its progenitor at the tip of the asymptotic giant branch.

B2.2 Schematic evolution of a binary

The evolution of a single isolated or unperturbed binary is carried out in the following steps (see Sections B2.3 and B2.4 for details).

A binary is ready to evolve after its orbital parameters are set, and the primary and secondary stars are identified. The first thing to do then is to determine the binary evolution time-step. This is the smallest time-step allowed by either of the stars. A stellar evolution time-step is 1 per cent of the time taken for the star to evolve from the start of one evolutionary stage to the next–for example, from the ZAMS to the terminal-age main sequence. (The stellar evolution step is not to exceed 1 Myr.) A list of these mileposts along a star's evolution is provided in Section B2.1. A binary is evolved whenever one of its stars requires an update. If a binary is in a state of mass transfer (but not in a common envelope) the time-step is reduced such that $\leq$1 per cent of the donor envelope is lost per step.

Each binary evolution step is subdivided into the following phases.

(i) Angular momentum loss (aml)

(a) by magnetic stellar wind,
(b) by gravitational wave radiation.

(ii) Check for coalescence.
(iii) Evolve primary star:

(a) adjust binary parameters for stellar wind mass-loss,
(b) resolve supernova.

(iv) Check if binary still exists. The evolution of the primary [or secondary, see (v)] star may have resulted in a supernova which may disrupt the binary or resulted in a collision between the two stars.
(v) Evolve secondary star:

(a) adjust binary parameters for stellar wind mass-loss,
(b) resolve supernova.

(vi) Check if binary still exists [see (iv)].
(vii) Check for tidal effects:

(a) circularize binary if appropriate (see Section B2.3),
(b) synchronize binary components if appropriate.

(viii) Check if any star is Roche lobe filling and identify the donor and the accretor. If neither star is filling its Roche lobe, leave binary evolution and notify dynamics, otherwise proceed with the following steps:

(a) find moment mass transfer starts,
(b) check binary stability:
– if binary unstable apply common envelope,
– if components merge leave binary evolution and notify dynamics,
(c) calculate $\zeta_{\rm ad}$, $\zeta_{\rm Rl}$ and $\zeta_{\rm th}$,
(d) determine amount of mass-loss from donor,
(e) determine amount of mass gained by accretor,
(f) subtract mass from donor,
(g) add mass to accretor, calculate new evolutionary state of accretor and rejuvenate (Section B2.4),
(h) calculate new binary parameters.
(i) determine the observational binary characteristics and stellar spectral types.

B2.3 Evolution of binary parameters without mass transfer

The orbital parameters of a binary are affected by the evolution of its components. We will not present here all the many details of binary evolution, but for clarity we summarize those which affect the dynamics or are important for interpreting our results. The details of the binary evolution program SeBa are discussed in more detail by Portegies Zwart & Verbunt (1996) and Portegies Zwart & Yungelson (1998).

Mass lost in a stellar wind is assumed to escape isotropically from the mass-losing star. If the companion accretes a fraction ξ of the other star's wind, this implies

$$\frac{a}{a_0} = f\frac{M_0+m_0}{M+m}, \tag{B15}$$

Here M_0 and m_0 are the initial primary and secondary mass, respectively, and M and m are their final masses. Also,

$$f = \left[\left(\frac{M}{M_0}\right)^{\xi}\frac{m}{m_0}\right]^{-2}. \tag{B16}$$

The fraction ξ is calculated via Bondi–Hoyle (1944) accretion, assuming that the thermal velocity in the wind equals the escape velocity of the mass-losing star (for details see Portegies Zwart & Verbunt 1996).

When the radius of one of the stars exceeds 5 times the orbital periastron separation $a(1-e)$, orbital energy is transformed into oscillatory modes in the two stars. This leads to a decrease in the orbital separation and, due to conservation of angular momentum [$a(1-e^2) = \text{constant}$], to the eventual circularization of the binary.

Mass-loss in a supernova takes place impulsively from the binary system. As a result, both the orbital separation and the eccentricity change: both increase if the pre-supernova orbit was circular. The velocity kick (equation B14) received by the neutron star at formation is added in a random direction to its orbital velocity. New orbital parameters are then calculated, assuming that the positions of the two stars are unchanged, that mass is lost isotropically from the exploding star, and that the companion is unaffected by the explosion. If the pre-supernova orbit is eccentric, things get somewhat more complicated (see Portegies Zwart & Verbunt 1996).

Low-mass stars may have magnetically coupled winds, and relatively large changes in angular momentum may occur even when a negligible amount of mass escapes. We follow the prescription described by Rappaport, Joss & Verbunt (1983) for

Table B1. Schematic diagram of the time-scales on which stable mass transfer (donor to accretor) proceeds.

Donor:	main sequence	subgiant	supergiant	compact object
Accretor:				
main-sequence	nuclear/thermal	thermal	dynamic	–
(sub)giant	–	nuclear/thermal	thermal/dynamic	–
compact object	thermal/aml	dynamic	dynamic	aml

Table B2. Free parameters in binary evolution.

term	value	description
κ	1	accretor rejuvenation factor
$\eta_{\rm J}$	2	specific angular momentum loss per unit mass
λ	0.5	envelope binding energy fraction
$\alpha_{\rm ce}$	4	common-envelope constant

tidally synchronized binaries in which at least one component is a main-sequence star or (sub)giant with mass $0.7 \leq m/{\rm M}_\odot \leq 1.5$.

Compact stars in short-period binaries and highly eccentric binaries lose orbital energy and angular momentum via gravitational radiation. For such binaries, we use the expressions provided by Peters (1964) to compute the time dependence of the orbital semimajor axis and eccentricity.

B2.4 Mass transfer in binaries

When one star in a binary approaches its Roche limit, we iteratively determine the moment at which contact occurs. The size of the Roche lobe is calculated as (Eggleton 1983)

$$r_{\rm Rl} = \frac{0.49}{0.6 + q^{2/3}\ln(1+q^{-1/3})}, \tag{B17}$$

where $q \equiv m/M$. The Roche lobe filling star is then identified as the donor, and its companion as the accretor.

B2.4.1 Unstable mass transfer. When a star fills its Roche lobe, we first check for the possibility of Darwin–Riemann instability. This happens if

$$J_{\rm donor} > \tfrac{1}{3} J_{\rm bin}, \tag{B18}$$

where $J_{\rm donor}$ and $J_{\rm bin}$ are the angular momenta of the Roche lobe-filling star and the binary, respectively.

During spiral-in the envelope of the donor is expelled, at the cost of orbital energy, following the prescription of Webbink (1984):

$$\frac{a}{a_0} = \frac{M_{\rm c}}{M}\left(\frac{1+2a_0}{\alpha\lambda}\frac{M_{\rm e}}{m}\right)^{-1}. \tag{B19}$$

The parameters governing binary evolution are listed in Table B2.

If the Roche lobe-filling star is a main-sequence star or compact object, the two stars simply merge because the donor has no core–halo structure. A merger occurs when the binary that remains after the common-envelope phase is semidetached, in which case no more mass is lost (see Section B4).

If the donor and the accretor are both (sub)giants and mass transfer happens to be dynamically unstable, we expel both envelopes at the cost of the binding energy of the binary in a *double spiral-in* (see Nelemans et al. 2000). The cores of the two giants will then spiral-in in the combined envelopes of the two (sub)giants. The energy required to expel the combined envelopes is computed by analogy with the standard common envelope (see equation B19). The final orbital separation is then be calculated by solving the energy balance between the orbital energy and the binding energies of both envelopes:

$$\frac{MM_{\rm e}}{\lambda R} + \frac{mm_{\rm e}}{\lambda' r} \equiv \alpha\left[\frac{M_{\rm c}m_{\rm c}}{2a} - \frac{(M_{\rm c}+M_{\rm e})(m_{\rm c}+m_{\rm e})}{2a_0}\right]. \tag{B20}$$

Here $m_{\rm e}$ and $m_{\rm c}$ are the envelope and core masses of the secondary star, where R and r are the radii of the two giants before the common envelope. We assume that the binding energy of both envelopes are the same, i.e., $\lambda' = \lambda$.

The double spiral-in results in a merger if the final orbital separation a is too small for in a semidetached binary with the two stellar cores. In this case, a fraction f of both stellar envelopes is lost from the binary system, and the rest $(1-f)$ is retained.

The merged star has a core mass equal to the sum of the cores of the two merged stars $(M_{\rm c}+m_{\rm c})$, and the envelope of the merged star has mass $(1-f)(M_{\rm e}+m_{\rm e})$, with $f \leq 1$. Instead of a total mass $M_{\rm e}+m_{\rm e}$, only $f(M_{\rm e}+m_{\rm e})$ is lost before the two stars merge. We can calculate f by solving equation (B20) with the envelope masses substituted for the amount of mass lost in the double spiral-in, i.e., $M_{\rm e}$, becomes $fM_{\rm e}$, and $m_{\rm e}$ becomes $fm_{\rm e}$. In order to solve this equation for f, we have to replace the final semimajor axis with the separation at which one of the cores start filling its Roche lobe.

B2.4.2 Stable mass transfer. We calculate the time-scale for mass transfer in a dynamically stable binary by considering the responses of the donor and the binary parameters to changes in the donor mass. For this purpose we define the logarithmic derivative

$$\zeta_{\rm i} = \left(\frac{{\rm d}\ln r}{{\rm d}\ln m}\right)_{\rm i}, \tag{B21}$$

for each of the following processes:

$\zeta_{\rm ad}$ the change in donor radius due to adiabatic adjustment of hydrostatic equilibrium,

$\zeta_{\rm Rl}$ the change in the size of the donor's Roche lobe,

$\zeta_{\rm th}$ the change in donor radius as it adjusts to a new thermal equilibrium.

The adopted values for $\zeta_{\rm ad}$ are as follows. For main-sequence stars with $m > 0.7\,{\rm M}_\odot$ and in the Hertzsprung gap we use $\zeta_{\rm ad} = 4$ and half this value for lower mass main-sequence stars. For stars on the horizontal branch we use $\zeta_{\rm ad} = 15$. For other stars with a core–halo structure (subgiants, supergiants and Thorne–Żytkow objects) we use the following fit to the composite polytropic models of Hjellming & Webbink (1987):

$$\zeta_{\rm ad} = -0.22 - 2.85x + 32.0x^2 - 75.7x^4 + 57.8x^5, \tag{B22}$$

where $x = m_c/m$.We use ζ_{th} between 0 and 0.9 for main-sequence stars and $\zeta_{th} = 0$ for all other stars, except those on the Hertzsprung gap and on the horizontal branch for which we use $\zeta_{th} = -2$ and 15, respectively.

The response of the Roche lobe to mass transfer ζ_{Rl} is calculated by transferring a infinitesimal amount of mass from the donor to the accreting star, and we study the response of the binary parameters. This test particle is transferred on the same time-scale as was used in the previous mass transfer step. At first Roche lobe contact, when there was no previous mass transfer step, we assume that the test particle is transferred on a thermal time-scale, which is a rather conservative choice.

The time-scale on which mass transfer proceeds is determined as follows:

$\zeta_{ad} < \zeta_{Rl}$ dynamically unstable mass transfer proceeds on time-scale τ_{dyn}

$\zeta_{ad} > \zeta_{Rl}$ and $\zeta_{th} < \zeta_{Rl}$ thermally unstable mass transfer proceeds on time-scale τ_{th}

$\zeta_{ad} > \zeta_{Rl}$ and $\zeta_{th} \geq \zeta_{Rl}$ nuclear unstable mass transfer proceeds on time-scale min (τ_{nuc}, τ_J),

where the time-scales associated with the various criteria are as follows:

dynamic : $\tau_{dyn} \simeq 5.1 \times 10^{-11} \sqrt{r^3/m}$[Myr]

thermal : $\tau_{th} \simeq 32m^2/(rL)$ [Myr]

nuclear : $\tau_{nuc} \simeq 0.1 t_{ms}$

aml : $\tau_J \simeq J_{bin}/(\dot{J}_{gr} + \dot{J}_{mb})$.

Here t_{ms} is a star's main-sequence lifetime, and m, r and L are its mass, radius and luminosity, respectively. The loss of angular momentum via gravitational radiation and magnetic braking are denoted by $\dot{J}_{gr}$ and $\dot{J}_{mb}$, respectively.

Table B1 gives a flavour of the various time-scales on which mass transfer generally proceeds. However, the details depend critically on the orbital separation and on the mass and evolutionary state of both the donor and the accreting star.

Some mass may be lost from the binary system during mass transfer. The new orbital parameters are calculated assuming that the mass lost from the binary carries specific angular momentum η_J (see Table B2). We calculate the final orbital separation using

$$\frac{a}{a_0} = \left(\frac{Mm}{M_0 m_0}\right)^{-2} \left(\frac{M+m}{M_0+m_0}\right)^{2\eta_J+1}. \quad \text{(B23)}$$

Here $M = M_0 - \mathrm{d}M$ and $m = m_0 + \mathrm{d}m$ (so $\mathrm{d}M$ and $\mathrm{d}m$ are defined as positive quantities). The binary thus loses mass if $\mathrm{d}M - \mathrm{d}m \geq 0$. For the amount of mass accepted by the accretor, see Portegies Zwart & Verbunt (1996).

B3 Rejuvenation of the accretor

An accreting star generally becomes more massive, which shortens its evolutionary time-scale. The method described here is rather ad hoc. We assume that a star accreting δm of mass remains in the same evolutionary state (see the list in Section B2.1). The age of the star with mass m is $t(m)$, and we want to know what is the age $t(m + \delta m)$ of the star with mass $m + \delta m$. At the moment the mass of the accretor increases from m to $m + \delta m$ the star is in evolutionary state i. It took the star $t_i(m)$ to reach that evolutionary state, and this state lasts for $\tau_i(m) \equiv t_{i+1}(m) - t_i(m)$ for a star with mass m. The same stage for a star with mass $m + \delta m$ lasts for $\tau_i(m + \delta m)$. The age of the star after accretion then becomes

$$t(m+\delta m) = t_i(m+\delta m) + \left[\frac{t(m) - t_i(m)}{\tau_i(m)}\right] \tau_i(m+\delta m)\mathcal{R}. \quad \text{(B24)}$$

Here $\mathcal{R}$ is a fraction introduced to mimic the rejuvenation of the accretor ($\mathcal{R} > 1$). The mass dumped on its surface may lead to some internal mixing, refreshing some of the helium core material with some of the freshly accreted hydrogen. This rejuvenation fraction is calculated with

$$\mathcal{R} = \left(\frac{m+\delta m}{m}\right)^{\kappa}, \quad \text{(B25)}$$

and we use $\mathcal{R} = 1$ if the accreted material is not hydrogen, in which case the accretor is not rejuvenated. Allowing $\mathcal{R} < 1$ would mimic the behaviour of a star becoming older upon accreting material. The adopted value for κ is listed in Table B2.

We will give two examples of an $m = 2\,\mathrm{M}_\odot$ star which accretes $\delta m = 0.2\,\mathrm{M}_\odot$ from a helium-rich companion ($\mathcal{R} = 1$). For simplicity, we assume here that this amount of mass is transferred in an infinitesimal time-step. The main-sequence lifetime for a 2-$\mathrm{M}_\odot$ star is about 801 Myr, and about 608 Myr for a 2.2-$\mathrm{M}_\odot$ star. If mass transfer starts at $t = 700$ Myr, the $2\,\mathrm{M}_\odot$ accretor is still on the main sequence. After mass transfer the accreting star has an age of 531 Myr and is still on the main sequence.

If mass transfer started at $t = 1$ Gyr, things become somewhat more complicated. The 2-$\mathrm{M}_\odot$ accretor is then on the horizontal branch. The time it takes from zero-age to the beginning of the horizontal branch is about 938 Myr; for a 2.2-$\mathrm{M}_\odot$ star this is about 712 Myr. The 2-$\mathrm{M}_\odot$ star spends roughly 84 Myr on the horizontal branch, whereas a 2.2-$\mathrm{M}_\odot$ star spends only 82 Myr in that stage. Substitution of these numbers into equation (B24) results in an age of the post-mass-transfer star of 773 Myr.

B4 RESULT OF A MERGER OR COLLISION

We have adopted a set of simple prescriptions to specify the outcome of stellar collisions. In the future these prescriptions can be refined when more accurate calculations become available. As a rule of the thumb, the result of a collision is the conservative accretion of the lower mass star on to the more massive star. The accretor will then be rejuvenated as described by equation (B25). This rule is violated when one component is a giant or a compact

Table B3. Simplified representation of possible merger outcomes. The four columns correspond to the four choices given for the type of massive star (primary), while the four rows indicate the type of less massive star (secondary): main-sequence star (ms), (sub)giant (sg), white dwarf (wd) and neutron star (ns). In this table we do not distinguish between stars in the Hertzsprung gap (Hg) or on the first and second ascent on the asymptotic giant branch (AGB).

	primary			
star	ms	sg	wd	ns
ms	ms	sg	wd + disc	ns + disc
sg	Hg	AGB	wd + disc	ns + disc
wd	sg	AGB	–	–
ns	TZO	TZO	–	–

object. A detailed prescription of how to calculate the evolutionary state of such a merger is presented in Paper I.

We describe our treatment of the possible outcomes of encounters between two stars, ordered by the evolutionary state of the more massive of the two (the primary). Table B3 summarizes this treatment.

B4.1 Main-sequence primary

If both stars involved in the encounter are main-sequence stars, then the less massive star is accreted conservatively on to the more massive star. The resulting star is a rejuvenated main-sequence star (see Lai, Rasio & Shapiro 1993 and Lombardi, Rasio & Shapiro 1995). The details of this procedure are described in appendix C4 of Portegies Zwart & Verbunt (1996).

If the less massive star in the encounter has a well-developed core (giant or subgiant), this core becomes the core of the merger product. The main-sequence star and the envelope of the giant are combined to form the new envelope of the merger. In general, the mass of the core is relatively small compared to the mass of the envelope, and the star is assumed to continue its evolution through the Hertzsprung gap. Note that this type of encounter can occur only when the main-sequence star is itself a collision product (e.g., a blue straggler).

When a main-sequence star encounters a less massive white dwarf, we assume that the merger product is a giant whose core and envelope have the masses of the white dwarf and the main-sequence star, respectively. We then determine its evolutionary state as follows. We calculate the total time $t_{\rm agb}$ that a single, unperturbed star with mass equal to that of the merged star would spend on the asymptotic giant branch, and the mass $m_{\rm c,agb}$ of its core at the tip of the giant branch. The age of the merger product is then calculated by adding $t_{\rm agb} m_{\rm c}/m_{\rm c,agb}$ to the age of an unperturbed star with the same mass at the bottom of the asymptotic giant branch. For example, a single, unperturbed 1.4-$M_\odot$ star leaves the main sequence after 2.52 Gyr, spends 60 Myr in the Hertzsprung gap, moves to the horizontal branch at 2.96 Gyr, and reaches the tip of the asymptotic giant branch after 3.06 Gyr, with a core of 0.64 $M_\odot$. Thus, if a 0.6-$M_\odot$ white dwarf merges with an 0.8-$M_\odot$ main-sequence star, the merger product has an age of 2.87 Gyr, leaving it another 180 Myr before it reaches the tip of the asymptotic giant branch.

If the less massive star is a neutron star or black hole, a Thorne–Żytkow object is formed.

B4.2 Evolved primary

When a (sub)giant or asymptotic branch giant encounters a less massive main-sequence star, the main-sequence star is combined with the envelope of the giant, which stays in the same evolutionary state. Its age within that state is changed, however, according to the rejuvenation calculation described in Section C3 of Portegies Zwart & Verbunt (1996). For example, an encounter of a giant of 0.95 $M_\odot$ and age 11.34 Gyr with a 0.45-$M_\odot$ main-sequence star produces a giant of 1.4 $M_\odot$ with an age of 2.67 Gyr.

When both stars are (sub)giants, the two cores are merged and form the core of the merger product (see Davies, Benz & Hills 1991 and Rasio & Shapiro 1995). Half the envelope mass of the less massive star is accreted on to the primary. The merger product continues its evolution starting at the next evolutionary state – a (sub)giant continues its evolution on the horizontal branch, and a horizontal branch star becomes an asymptotic giant branch star. The reasoning behind this assumption is that an increased core mass corresponds to a later evolutionary stage.

If the less massive star is a white dwarf, then its mass is simply added to the core mass of the giant, and the envelope is retained. If the age of the giant before the encounter exceeds the total lifetime of a single unperturbed star with the mass of the merger, then the newly formed giant immediately sheds its envelope and its core turns into a single white dwarf. Otherwise the merged giant is assumed to have the same age (in years) as the giant before the collision, and continues its evolution as a single unperturbed star.

If the other star is a less massive neutron star, a Thorne–Żytkow object is formed.

B4.3 White-dwarf primary

In an encounter between a white dwarf and a less massive main-sequence star, the latter is assumed to be completely disrupted, and forms a disc around the white dwarf (Ruffert & Müller 1990; Rasio & Shapiro 1991). The white dwarf accretes from this disc at a rate of 1 per cent of the Eddington limit. If the mass in the disc exceeds 5 per cent of the mass of the white dwarf, the excess mass is expelled from the disc at a rate equal to the Eddington limit.

If a white dwarf encounters a less massive (sub)giant, a new white dwarf is formed with a mass equal to the sum of the pre-encounter core of the (sub)giant and the white dwarf. The newly formed white dwarf is surrounded by a disc formed from half the envelope of the (sub)giant before the encounter. The factor of a half is rather arbitrary and based on the lack of detailed calculations which provide a proper number. If the mass of the white dwarf exceeds the Chandrasekhar limit, it explodes in a type Ia supernova, leaving no remnant (Nomoto & Kondo 1991; Livio & Truran 1992).

A collision between two white dwarfs results in a single white dwarf with mass equal to the sum of the original masses. If the total mass of the collision product exceeds the Chandrasekhar mass, it explodes in a type Ia supernova.

Collisions between white dwarfs and neutron stars or black holes result in the formation of an accretion disc around the compact object; the white dwarf is destroyed. Following the accretion, the neutron star may collapse into a black hole.

B4.4 Neutron-star or black-hole primary

All collisions involving a neutron-star or black-hole primary lead to the formation of a massive disc around the compact star. If the compact star had a disc prior to the collision, this disc is expelled. This disc accretes on to the compact star. We chose, rather arbitrarily, that the accretion rate is 5 per cent of the Eddington limit. An accreting neutron star turns into a millisecond radio pulsar, or – when its mass exceeds 2 $M_\odot$ – into a black hole.

B5 COMMUNICATION BETWEEN SEBA AND KIRA

Due to the interaction between stellar evolution and stellar dynamics, it is difficult to solve for the evolution of both systems in a completely self-consistent way. The trajectories of stars are computed using a block time-step scheme, as described earlier. Stellar and binary evolution is updated at fixed intervals (every 1/64 of a crossing time, typically a few thousand years). Any feedback between the two systems may thus experience a delay of

at most one time-step. Internal evolution time steps may differ for each star and binary, and depend on binary period, perturbations due to neighbours, and the evolutionary state of the star. Time-steps in this treatment vary from several milliseconds up to (at most) a million years.

After each 1/64 of a crossing time, all stars and binaries are checked to determine if evolutionary updates are required. Single stars are updated every 1/100 of an evolution time-step or when the mass of the star has changed by more than 1 per cent since the last update. A stellar evolution time-step is the time taken for the star to evolve from the start of one evolutionary stage to the next (see Section B2.2).

After each stellar evolution step the dynamics is notified of changes in stellar radii, but changes in mass are, for reasons of efficiency, not passed back immediately (mass changes generally entail recomputing the accelerations of all stars in the system). Instead, the 'dynamical' masses are modified only when the mass of any star has changed by more than 1 per cent, or if the orbital parameters, semimajor axis, eccentricity, total mass or mass ratio of any binary has changed by more than 0.1 per cent.

B6 MASS-LOSS FROM STARS AND BINARIES

Fast (sudden) and slow (gradual) mass-loss affects the dynamics of the stellar system in different ways. Mass-loss is considered fast when it takes place within a fraction of an orbital time-scale. For single stars, this time-scale is of the order of the crossing time of the star cluster. For binaries, it is much shorter–on the order of the binary orbital period. Mass-loss during a supernova explosion is considered fast, stellar winds and mass lost from a binary during mass transfer are considered slow.

Due to the discretized time steps of the stellar dynamics and the stellar evolution, from the point of view of the dynamics mass is lost in 'bursts'. For example, an asymptotic giant branch star with a strong stellar wind may lose its entire envelope in 100 steps spanning roughly one crossing time, while a supergiant might lose its entire envelope instantaneously in a supernova. Mass-loss for single stars affects the dynamics of the entire stellar system. For binaries and multiple systems, mass-loss from a member star directly affects the orbital characteristics of its neighbours.

The rate of mass-loss is particularly important for binaries. Slow mass-loss via a stellar wind will soften a binary system, but will not affect its eccentricity or its centre-of-mass velocity. (This is true if the binary is unperturbed. In a perturbed binary, the eccentricity and centre of mass velocity are both affected by stellar wind mass-loss.) Sudden mass-loss, on the other hand, can dramatically affect the binary's internal parameters. For unperturbed binaries, the effects of mass-loss from both component stars are computed consistently using SeBa. Changes in binary parameters are calculated and the dynamics is notified, thereby transmitting the information to the rest of the stellar system via the integrator.

For perturbed binaries and multiples (and also hierarchical systems where the inner binary is unperturbed), the integrator takes care of the dynamical effects of stellar mass-loss. By construction, mass transfer cannot occur in a perturbed binary or multiple system. If a supernova occurs in a perturbed binary, any slow mass-loss is accounted for before fast mass-loss occurs, since a star which is about to explode generally loses a significant fraction of its mass in a stellar wind before the supernova event itself. Supernova remnants do not lose mass. This assumption breaks down when the binary companion of the exploding star loses a significant fraction of its mass between the moment of the supernova and the end of the stellar update time-step. (This can happen if the binary companion is either a hypergiant, a massive helium star or a supergiant.) The stellar evolution time steps in these cases are taken sufficiently small (on the order of 100 years) to ensure that this causes a negligible error.

B7 COLLISIONS AND MERGERS

We draw a distinction between 'mergers' and 'collisions.' A merger may result from mass transfer or a common-envelope phase during the evolution of an unperturbed binary. The binary node is then replaced by the merger product. The product of a merger is generally different from the result of a collision, since a merger is often preceded by a phase of mass transfer which affects the masses of both stars.

Collisions may occur between single stars (which are part of a binary tree) or between stars in a perturbed binary. Since the integrator may miss the precise moment of closest approach, the orbital elements of each 'close' pair of stars is calculated after each integration step. A collision occurs when the stars are found to be within $d_{\rm coll}$ times the sum of their radii at periastron: $p < d_{\rm coll}(r_1 + r_2)$. In this case, the two stars are replaced by the collision product, which is placed at the centre of mass and with the centre-of-mass velocity of the original two-body system. The characteristics of the collision product are calculated using SeBa (Section B4).

A collision may also occur when an unperturbed binary in a state of mass transfer is perturbed by a close encounter with another cluster member. Such a induced collision may be triggered by a close flyby, or in a multiple system with a perturbed outer orbit. The collision occurs if the sum of the component radii exceeds the distance between the two stars at the moment the binary becomes perturbed.

This paper has been typeset from a TEX/LATEX file prepared by the author.